Helical turbulent Prandtl number in the A model of passive vector advection

M. Hnatič[1,2,3] and P. Zalom[2,3]
[1]*Faculty of Sciences, P.J. Safarik University, Košice, Slovakia*
[2]*Institute of Experimental Physics, SAS, Watsonova 47, 040 01 Košice, Slovakia*
[3]*Bogoliubov Laboratory of Theoretical Physics, Joint Institute for Nuclear Research, 141 980 Dubna, Moscow Region, Russian Federation*
(Received 15 May 2016; published 16 November 2016)

Using the field theoretic renormalization group technique in the two-loop approximation, turbulent Prandtl numbers are obtained in the general A model of passive vector advected by fully developed turbulent velocity field with violation of spatial parity introduced via the continuous parameter ρ ranging from $\rho = 0$ (no violation of spatial parity) to $|\rho| = 1$ (maximum violation of spatial parity). Values of A represent a continuously adjustable parameter which governs the interaction structure of the model. In nonhelical environments, we demonstrate that A is restricted to the interval $-1.723 \leqslant A \leqslant 2.800$ (rounded to 3 decimal places) in the two-loop order of the field theoretic model. However, when $\rho > 0.749$ (rounded to 3 decimal places), the restrictions may be removed, which means that presence of helicity exerts a stabilizing effect onto the possible stationary regimes of the system. Furthermore, three physically important cases $A \in \{-1,0,1\}$ are shown to lie deep within the allowed interval of A for all values of ρ. For the model of the linearized Navier-Stokes equations ($A = -1$) up to date unknown helical values of the turbulent Prandtl number have been shown to equal 1 regardless of parity violation. Furthermore, we have shown that interaction parameter A exerts strong influence on advection-diffusion processes in turbulent environments with broken spatial parity. By varying A continuously, we explain high stability of the kinematic MHD model ($A = 1$) against helical effects as a result of its proximity to the $A = 0.912$ (rounded to 3 decimal places) case where helical effects are completely suppressed. Contrary, for the physically important $A = 0$ model, we show that it lies deep within the interval of models where helical effects cause the turbulent Prandtl number to decrease with $|\rho|$. We thus identify internal structure of interactions given by the parameter A, and not the vector character of the admixture itself being the dominant factor influencing diffusion-advection processes in the helical A model.

DOI: 10.1103/PhysRevE.94.053113

I. INTRODUCTION

Diffusion-advection processes in turbulent environments represent both experimentally and theoretically an important topic of study in the field of fluid motion [1–5]. In this respect, the so-called Prandtl number is frequently used to compactly characterize the quantitative properties of flows under the study [2,3]. For all admixture types, it is defined as the dimensionless ratio of the coefficient of kinematic viscosity to the corresponding diffusion coefficient of a given admixture. For example, in the case of thermal diffusivity, the corresponding (scalar) Prandtl number equals the ratio of kinematic viscosity to the coefficient of molecular diffusivity [3]. Since both the kinematic viscosity and the diffusion coefficient for the given admixture are material and flow specific quantities, the resulting Prandtl numbers have always to be specified at distinct conditions required to characterize the flow and are thus often found in property tables alongside with other material specific properties [1,2,6,7].

However, in the high Reynolds number limit, the state of fully developed turbulence manifests itself by reaching effective material and flow independent values for both the kinematic viscosity and the corresponding diffusion coefficient. We commonly refer to such effective values as the turbulent viscosity coefficient and turbulent diffusion coefficient [3,4]. Consequently, in fully developed turbulent flows the resulting values of the Prandtl numbers are universal for a given admixture and do not depend either on microscopic or macroscopic properties of the flow under the consideration. Usually, we refer to them as the turbulent Prandtl numbers of given admixture type [1,2,8,9].

In other words, the state of fully developed turbulence allows study of advection-diffusion processes in a general material and flow unbiased manner [3,4]. Moreover, it is well known that fully developed turbulent systems are well tractable for analytic investigations which would otherwise be difficult or even impossible [9,10]. Fully developed turbulent flows represent therefore a theoretically as well as experimentally valuable scenario for analytic studies of how different admixtures are transported within the underlying turbulent environment.

In this respect, several authors have recently analyzed the question of how the tensorial nature of the admixtures under consideration may alter the diffusion-advection processes [11–15]. As a starting point for the present analysis, we briefly discuss Refs. [11,15] where the aforementioned turbulent Prandtl was central in the approach to the problem. In Ref. [15], turbulent scalar Prandtl number was investigated in the model of passive advection while in Ref. [11] two other models, namely, the so-called kinematic MHD model and a passively advected vector field within the $A = 0$ model, were included into the analysis. Furthermore, the authors of Ref. [11] show that introduction of spatial parity violation (helicity) into the turbulent flow represents not only a highly realistic physical scenario, but it additionally has the advantage of pronouncing differently the specific tensorial and interaction properties of the studied models from which the authors argue that the structure of interactions exerts more impact on diffusion-advection processes than the tensorial nature of the advected field itself. The drawback of the analysis performed in Ref. [11] lies in the fact that interactions in

the given models could not be varied in any way. Extending the results beyond the three selected models represents thus merely a hypothesis. However, two of the analyzed models, namely, the kinematic MHD model and the aforementioned $A = 0$ model represent special cases of the general A model of passive vector advection as first defined in Ref. [16]. To avoid confusion, we stress that the present general A model is restricted only to the passive vector advection and it should not be confused with the A model according to the classification of Halperin and Hohenberg [18] or with the A model of forced Navier-Stokes equation introduced in Refs. [19,20]. The name of the present model is actually drawn from the commonly used notation for the parameter A [11–17,21] which appears in its definition (see Sec. II for more details). The parameter A plays actually a central role in an appropriate definition of a unified description of a wide variety of vector admixture models. Since it is only required to be real with no further restrictions being obvious, it may take values of $A = 1$ and 0 which give the kinematic MHD model and the $A = 0$ model, respectively. Moreover, it also encompasses the important case of the so-called linearized Navier-Stokes equations [21]. Thus, the general A model represents a tool to unite several distinct but physically important cases into one single model. However, as already seen in Ref. [16], further restrictions on A may arise and we discuss those in Sec. V.

A step towards the aforementioned generalization was already undertaken in Ref. [14]. However, only the case of fully symmetric turbulent environment was considered and, consequently, only limited insights into the problem was gained. Without considering helical effects, assertions made by the authors of Ref. [11] remained therefore completely unverified. It is therefore of high interest to include spatial parity violation into the general A model. Additionally, the authors of Ref. [14] constraint the values of A only to the interval $\langle -1,1\rangle$ and omit the important physical cases beyond the limit of their analysis. Taking together, although the general A model has attracted a lot of attention recently (see Refs. [12,13,21]), only the case of fully symmetric turbulent environment has been analyzed so far. Furthermore, the analysis has been limited only onto the values $-1 \leqslant A \leqslant 1$ case. Here, we consider the general helical case and further extend the calculations to all physically allowed values of A.

To perform the investigations discussed above, we use the well established tools of the field renormalization group (RG) technique, as presented, for example, in Refs. [9,10,22], which was widely used in the field of fully developed turbulence without admixtures [23–29] as well as for advection-diffusion processes of several admixtures including passive scalar admixture [15,30–35], magnetic admixtures [36–40], and also vector admixtures [11–14,21,41–44]. The two-loop techniques for calculation of the turbulent Prandtl number within the A model used here are similar to those of Ref. [15]. The resulting helical values of turbulent Prandtl number are then analyzed to finally investigate the hypothesis raised in Ref. [11].

The paper is structured as follows. In Sec. II, the A model of passive advection of the vector admixture is defined via the stochastic differential equations. The emphasis is laid on the meaning of the parameter A for the structure of interactions. In Sec. III, field theoretic equivalent of stochastic differential equations of the A model is introduced. The UV renormalization of the model is discussed in Sec. IV which is then concluded with the calculation of the IR stable fixed point of the basic RG equations. The two-loop calculation of the helical Prandtl number is presented in Sec. V where also the helical dependence of the turbulent Prandtl number is discussed with special attention given to the influence of tensorial interaction structures on the diffusion-advection processes in the A model studied here. Obtained results are then briefly reviewed in Sec. VI.

II. MODEL *A* OF PASSIVE VECTOR ADVECTION WITH SPATIAL PARITY VIOLATION

We consider a passive solenoidal vector field $\mathbf{b} \equiv \mathbf{b}(x)$ driven by a helical turbulent environment given by an incompressible velocity field $\mathbf{v} \equiv \mathbf{v}(x)$ where $x \equiv (t,\mathbf{x})$ with t denoting the time variable and $\mathbf{x}$ the d dimensional spatial position (later $d = 3$ strictly). Apparently, $\mathbf{v}$ and $\mathbf{b}$ are the divergence free vector fields satisfying $\partial \cdot \mathbf{b} = \partial \cdot \mathbf{v} = 0$. Additionally, within the general A model of passive advection the following system of stochastic equations is required:

$$\partial_t \mathbf{b} = \nu_0 u_0 \triangle \mathbf{b} - (\mathbf{v}\cdot\partial)\mathbf{b} + A(\mathbf{b}\cdot\partial)\mathbf{v} - \partial P + \mathbf{f}^b, \quad (1)$$

$$\partial_t \mathbf{v} = \nu_0 \triangle \mathbf{v} - (\mathbf{v}\cdot\partial)\mathbf{v} - \partial Q + \mathbf{f}^v, \quad (2)$$

where $\partial_t \equiv \partial/\partial_t$, $\partial_i \equiv \partial/\partial_{x_i}$, $\Delta \equiv \partial^2$ is the Laplace operator, ν_0 is the bare viscosity coefficient, u_0 is the bare reciprocal Prandtl number, $P \equiv P(x)$ and $Q \equiv Q(x)$ represent the pressure fields while the stochastic terms $\mathbf{f}^v$, $\mathbf{f}^b$ and the parameter A are discussed later in this section. The subscript 0 denotes unrenormalized quantities in what follows (see Sec. IV for more details).

Let us now briefly review the physical meaning of A. First, we note that Galilean symmetry requires A only to be real but the cases $A \in -1,0,1$ represent various physically important models [14,21,41,43]. For $A = 1$, the kinematic MHD model is recovered, the $A = 0$ case leads to passive advection of a vector field in turbulent environments, and finally $A = -1$ represents the model of the linearized Navier-Stokes equations [21]. The parameter A stands in front of the so-called stretching term [41] and due to its continuous nature it represents a measure of specific interactions allowed by Galilean symmetry. Varying A allows therefore to investigate a variety of passively advected vector admixtures with different interaction properties. Although A may take any real values, it is frequently discussed only in the smallest possible continuous interval encompassing the three special cases $A \in \{-1,0,1\}$. Contrary, we extend the analysis to all physically allowed values of A (see Sec. V for more details) which allows a straightforward discussion of the influence of interactions on advection-diffusion processes.

The previously undefined stochastic terms $\mathbf{f}^v$ and $\mathbf{f}^b$ introduced in Eqs. (1) and (2) represent sources of fluctuations for $\mathbf{v}$ and $\mathbf{b}$. For energy injection of $\mathbf{b}$ we assume transverse Gaussian random noise $\mathbf{f}^{\mathbf{b}} = \mathbf{f}^{\mathbf{b}}(x)$ with zero mean via the following correlator:

$$D^b_{ij}(x;0) \equiv \left\langle f^b_i(x) f^b_j(0)\right\rangle = \delta(t) C_{ij}(|\mathbf{x}|/L), \quad (3)$$

where L is an integral scale related to the corresponding stirring of $\mathbf{b}$ while C_{ij} is required to be finite in the limit $L \to \infty$ and for $|x| \gg L$ it should rapidly decrease, but remains otherwise unspecified in what follows. Contrary, the transverse random force per unit mass $\mathbf{f}^{\mathbf{v}} = \mathbf{f}^{\mathbf{v}}(x)$ simulates the injection of kinetic energy into the turbulent system on large scales and must suit the description of real infrared (IR) energy pumping. To allow the later application of the RG technique, we shall assume a specific, powerlike form of injection as usual for fully developed turbulence within the RG approach (for more details, see Refs. [9,10,27]). Nevertheless, although a specific form is used, universality of fully developed turbulence ensures that the results obtained here may easily be extended to all fully developed turbulent flows. Additionally, it allows easy generalization to environments with broken spatial parity by defining suitable tensorial properties of the correlator of $\mathbf{f}^{\mathbf{v}}$. For this purpose, we prescribe the following pair correlation function with Gaussian statistics:

$$D^v_{ij}(x;0) \equiv \left\langle f^v_i(x) f^v_j(0) \right\rangle = \delta(t) \int \frac{d^d\mathbf{k}}{(2\pi)^d} D_0 k^{4-d-2\varepsilon} R_{ij}(\mathbf{k}) e^{i\mathbf{k}\cdot\mathbf{x}}. \quad (4)$$

Here, d denotes the spatial dimension of the system, $\mathbf{k}$ is the wave number with $k = |k|$, and $D_0 \equiv g_0 \nu_0^3 > 0$ is the positive amplitude with g_0 being the coupling constant of the present model related to the characteristic ultraviolet (UV) momentum scale Λ by the relation $g_0 \simeq \Lambda^{2\varepsilon}$. The term $R_{ij}(k)$ appearing in Eq. (4) encodes the spatial parity violation of the underlying turbulent environment and its detailed structure is discussed separately in the text below. Finally, the parameter ε is related to the exact form of energy injection at large scales and assumes a value of 2 for physically relevant infrared energy injection. However, as usual in the RG approach to the theory of critical behavior, we treat ε formally as a small parameter throughout the whole RG calculations and only in the final step its physical value of 2 is inserted [9,22].

Further, in Eq. (4), we encounter typical momentum integrations which lead to two troublesome regions, namely, the IR region of low momenta and the UV region of high momenta as discussed in detail in Refs. [9,10]. Frequently, these troublesome integration regions are avoided by directly prescribing all relevant microscopic and macroscopic properties of the flow. Here, however, we use the universality of fully developed turbulent flows to avoid unnecessary specifications. Thus, we only demand real IR energy injection of energy via Eq. (4) and neglect the exact macroscopic structure of the flow by introducing a sharp IR cutoff $k \geqslant m$ for integrations over $\mathbf{k}$ with L assumed to be much bigger than $1/m$. Using sharp cutoff, IR divergences like those in Eq. (4) are avoided. As already done for Eq. (4), the IR cutoff is understood implicitly in the whole paper and we shall stress its presence only at the most crucial stages of the calculation. Contrary, UV divergences and their renormalization play the central role in calculations presented here.

Finally, let us now turn our attention to the projector R_{ij} in Eq. (4) which controls all of the properties of the spatial parity violation in the present model. In the case of fully symmetric isotropic incompressible turbulent environments, the projector $R_{ij}(k)$ assumes the usual form of the ordinary transverse projector

$$P_{ij}(\mathbf{k}) = \delta_{ij} - k_i k_j / k^2, \quad (5)$$

as explained in Ref. [9] in more details. In the case of helical flows with spatial parity violation, Eq. (4) is specified in the form of a mixture of a tensor and a pseudotensor as $R_{ij}(k) = P_{ij}(k) + H_{ij}(k)$ where $H_{ij}(k)$ respects the transversality of the present fields. The ordinary nonhelical transverse projector P_{ij} is thus shifted by a helical contribution

$$H_{ij}(\mathbf{k}) = i\rho\, \varepsilon_{ijl} k_l / k. \quad (6)$$

Here, ϵ_{ijl} is the Levi-Civita tensor of rank 3, and the real valued helicity parameter ρ satisfies $|\rho| < 1$ due to the requirement of positive definiteness of the correlation function. Obviously, $\rho = 0$ corresponds to the fully symmetric (nonhelical) case whereas $\rho = 1$ means that spatial parity is fully broken.

We finally conclude the section by discussing the structure of interactions in Eqs. (1) and (2). Obviously, according to Eq. (2), the admixture field $\mathbf{b}$ does not disturb evolution of the velocity field $\mathbf{v}$. In other words, the velocity field $\mathbf{v}$ is completely detached from the influence of admixtures, as required by demanding passive advection. Of course, real problems usually involve at least some small amount of mutual interaction between the flow and its admixtures. However, even in the case of active admixtures there exist regimes which correspond to the passive advection problem, as seen, for example, in the case of the MHD problem with an active magnetic admixture which has the so-called kinetic regime controlled by the kinematic fixed point of the RG equations (see, e.g., Ref. [36]). Such a situation corresponds to the passive advection obtained within the present model when $A = 1$ in Eqs. (1) and (2). Therefore,the present picture of passive advection within the A model represents a highly interesting physical scenario.

III. FIELD THEORETIC FORMULATION OF THE MODEL

According to the Martin-Sigia-Rose theorem [45], the system of stochastic differential equations (1) and (2) is equivalent to a field theoretic model of the double set of fields $\Phi = \{\mathbf{v},\mathbf{b},\mathbf{v}',\mathbf{b}'\}$ where primed fields are the auxiliary response fields [9]. The field theoretic model is then defined via the Dominicis-Janssen action functional

$$\begin{aligned} S(\Phi) = {} & \frac{1}{2} \int dt_1\, d^d\mathbf{x}_1\, dt_2\, d^d\mathbf{x}_2 \\ & \times \left[v'_i(x_1) D^v_{ij}(x_1;x_2) v'_j(x_2) + b'_i(x_1) D^b_{ij}(x_1;x_2) b'_j(x_2) \right] \\ & + \int dt\, d^d\mathbf{x} \{ \mathbf{v}'[-\partial_t + \nu_0 \triangle - (\mathbf{v}\cdot\partial)]\mathbf{v} \\ & + \mathbf{b}'[-\partial_t \mathbf{b} + \nu_0 u_0 \triangle \mathbf{b} - (\mathbf{v}\cdot\partial)\mathbf{b} + A(\mathbf{b}\cdot\partial)\mathbf{v}] \}, \end{aligned} \quad (7)$$

where $x_l = (t_l, \mathbf{x}_l)$ with $l = 1,2$, D^b_{ij} and D^v_{ij} are given in Eqs. (3) and (4), respectively, and the required summations over dummy indices $i,j \in 1,2,3$ are implicitly assumed. The auxiliary fields and their original counterparts $\mathbf{v}, \mathbf{b}$ share the same tensor properties, which means that all fields appearing in the present model are transverse. The pressure terms ∂Q and ∂P from Eqs. (1) and (2), respectively, do not appear in action (7) because transversality of the auxiliary fields $\mathbf{v}'(x)$

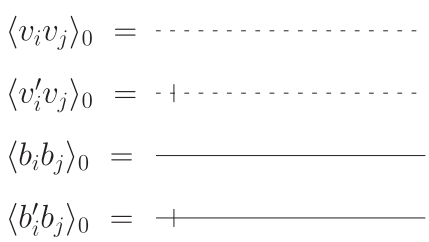

FIG. 1. Propagators of the general A model. Dashed lines correspond to fields $\mathbf{v}$ and $\mathbf{v}'$ while full lines denote fields $\mathbf{b}$ and $\mathbf{b}'$. Slash denotes auxiliary fields $\mathbf{v}'$ and $\mathbf{b}'$.

and $\mathbf{b}'(x)$ allows one to integrate these out of the action (7) by using the method of partial integration.

The field theoretic model of Eq. (7) has a form analogous to the corresponding expression of Ref. [14] but includes via D^v_{ij} the more general helical situation which was not considered by the authors of Ref. [14]. In the frequency-momentum representation, the following set of bare propagators is obtained:

$$\langle b'_i b_j \rangle_0 = \langle b_i b'_j \rangle^*_0 = \frac{P_{ij}(\mathbf{k})}{i\omega + \nu_0 u_0 k^2}, \tag{8}$$

$$\langle v'_i v_j \rangle_0 = \langle v_i v'_j \rangle^*_0 = \frac{P_{ij}(\mathbf{k})}{i\omega + \nu_0 k^2}, \tag{9}$$

$$\langle b_i b_j \rangle_0 = \frac{C_{ij}(\mathbf{k})}{|-i\omega + \nu_0 u_0 k^2|^2}, \tag{10}$$

$$\langle v_i v_j \rangle_0 = \frac{g_0 \nu_0^3 k^{4-d-2\varepsilon} R_{ij}(\mathbf{k})}{|-i\omega + \nu_0 k^2|^2}, \tag{11}$$

with helical effects already appearing in the propagator (11) via $R_{ij}(\mathbf{k})$. The function $C_{ij}(k)$ is the Fourier transform of $C_{ij}(r/L)$ from Eq. (3), but remains arbitrary in the calculations that follow. The propagators are represented as usual by the dashed and full lines, where the dashed lines involve the velocity type of fields and full lines represent the vector admixture type fields. The auxiliary fields are denoted using a slash in the corresponding propagators as shown in Fig. 1.

The field theoretic formulation of the A model contains also two different triple interaction vertices (see Fig. 2), namely, $b'_i(-v_j\partial_j b_i + A b_j \partial_j v_i) = b'_i v_j V_{ijl} b_l$ and $-v'_i v_j \partial_j v_i = v'_i v_j W_{ijl} v_l/2$. In the momentum-frequency representation, $V_{ijl} = i(k_j \delta_{il} - A k_l \delta_{ij})$ while $W_{ijl} = i(k_l \delta_{ij} + k_j \delta_{il})$. In both cases, momentum $\mathbf{k}$ is flowing into the vertices via the auxiliary fields $\mathbf{b}'$ and $\mathbf{v}'$, respectively. In the end, let us also briefly remind that the formulation of the stochastic

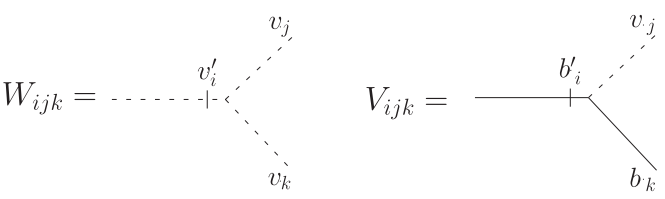

FIG. 2. The interaction vertices of the A model. The vertex $W_{ijk} = i(k_k \delta_{ij} + k_j \delta_{ik})$ involves the fields $\mathbf{v}$ and $\mathbf{v}'$ while V_{ijk} is the only diagrammatic object of the present Feynman rules which contains A dependent contribution in the form of $V_{ijk} = i(k_j \delta_{ik} - A k_k \delta_{ij})$.

problem given by Eqs. (1) and (2) through the field theoretic model with the action functional (7) allows one to use the well-defined field theoretic means, e.g., the RG technique, to analyze the problem [9,46].

IV. RENORMALIZATION GROUP ANALYSIS

To determine all relevant UV divergences in the present model, we employ the analysis of canonical dimensions and identify all objects (graphs) containing the so-called superficial UV divergences which turn out to be the only relevant divergences left for the subsequent RG analysis performed here (for details, see Refs. [9,10,22]). Since the present A model belongs to the class of the so-called two scale models [9,10,27], an arbitrary quantity Q has a canonical dimension $d_Q = d^k_Q + d^\omega_Q$, where d^k_Q corresponds to the canonical dimension in the momentum scale while d^ω_Q corresponds to the frequency scale. A straightforward calculation shows that for the helical parameter ρ one obtains $d^k_\rho = d^\omega_\rho = 0$ while all the other quantities possess canonical dimensions according to Ref. [14]. Consequently, the helical A model possesses dimensionless coupling constant g_0 at $\varepsilon = 0$.

The present model is thus logarithmic at $\varepsilon = 0$ which in the framework of the minimal subtraction (MS) scheme, as used here, means that all possible UV divergences are of the form of poles in ε [22,46]. Using now the general expression for the total canonical dimension of an arbitrary 1-irreducible Green's function $\langle \Phi \dots \Phi \rangle_{1-ir}$ and the symmetry properties of the model, one finds that for $d = 3$ the superficial UV divergences are present only in the 1-irreducible Green functions $\langle v'_i v_j \rangle_{1-ir}$ and $\langle b'_i b_j \rangle_{1-ir}$. Thus, all divergences can be removed by the counterterms of the form $\mathbf{v}'\Delta\mathbf{v}$ or $\mathbf{b}'\Delta\mathbf{b}$ which leads to the multiplicative renormalization of g_0, u_0, and ν_0 via

$$\nu_0 = \nu Z_\nu, \quad g_0 = g\mu^{2\varepsilon} Z_g, \quad u_0 = u Z_u, \tag{12}$$

where the dimensionless parameters g, u, and ν are the renormalized counterparts of the corresponding bare ones and μ is the renormalization mass required for the dimensional regularization, as used in this paper. The quantities $Z_i = Z_i(g,u;d,\rho;\varepsilon)$ contain poles in ε.

Furthermore, we stress that A is a free parameter in the model and is not renormalized as opposed to the charges listed in Eq. (12). This feature was already observed in Ref. [14] where a nonhelical equivalent of our model is investigated. On the other hand, when the correlations of the velocity field $\mathbf{v}$ are prescribed synthetically, as done for example in Refs. [16,17], parameter A cannot be freely adjusted. In such models, A becomes a charge of the model which for incompressible flows leads to only three allowed renormalized values of $1, 0, -1$ [17]. Moreover, when compressibility is present, the parameter A is renormalized only to a nonzero values of $1, -1, \alpha$ where α is a parameter describing compressibility [for details see Eq. (2.5) in Ref. [17]]. However, such consequences are attributed to $\mathbf{v}$ being prescribed synthetically by its two point correlator. We avoided such synthetic definitions by using stochastic Navier-Stokes equation to describe the evolution of $\mathbf{v}$. This scenario is not only more physical but, additionally, it has the benefit of A being a free parameter of the present model.

However, there exists an additional problem when passing from the nonhelical to the general parity broken A model.

Strictly speaking, the above conclusions are completely true only in the nonhelical case. In the general helical case, linear divergences in the form of $\mathbf{b}' \cdot \mathrm{curl}\,\mathbf{b}$ (also referred to as the curl term in this paper) appear in the 1-irreducible Green's function $\langle b'_i b_j \rangle_{1-ir}$; see Ref. [37] for more details. As it is very well known, the presence of the curl term for the $A = 1$ case leads to an exponential increase of magnetic fluctuations at large scales with subsequent instabilities emerging in the model [47,48]. In the steady state, these instabilities are generally attributed to the generation of large-scale magnetic field via the mechanism known as the turbulent dynamo (see, e.g. [49,50]). Successful incorporation of such a mechanism into the field theoretical description was performed by authors of Ref. [37] by introducing spontaneous symmetry breaking into the model. Technically, the original field $\mathbf{b}$, which describes magnetic fluctuations around zero mean magnetic field $\langle \mathbf{b} \rangle \equiv \mathbf{B} = 0$, was substituted by $\mathbf{b} + \mathbf{B}$ with $\mathbf{B}$ allowed to be nonzero.

The field $\mathbf{B}$ provides then all necessary means for the elimination of the curl term in the model; for details see Ref. [37]. It should be emphasized once again that in Ref. [37] the mechanism of spontaneous symmetry breaking is introduced only for the MHD model ($A = 1$) with Lorentz force term explicitly considered. In the field theoretical formulation, the added Lorentz term gives then subsequently rise to a new interaction term $\mathbf{b}'(\mathbf{b}\partial)\mathbf{b}$ in the action functional. Its presence is crucial for the elimination of curl divergences by employing the mechanism of spontaneous generation of the homogeneous magnetic field as described above.

Before proceeding further with the kinematic approximation, let us explain how one extends the mechanism of Ref. [37] from its special case $A = 1$ to the arbitrary values of A as considered in our paper. For such a purpose, one temporarily introduces a Lorentz-type term $b_i \partial_i b_j$ into the Navier-Stokes equation (2). The magnitude $|B|$ of the spontaneously generated field (with an arbitrary direction) follows then from the condition of cancellation of the curl term as discussed above. Thus, the field $\mathbf{B}$ depends explicitly on the parameter A in the general case. Moreover, some values of the parameter A may violate the condition of $|B|$ being positive which restricts the interval of admissible values of A. All of these facts are easily demonstrated by considering the special case of $A = -1$. Here, no curl terms emerge due to the appearance of symmetrical vertex in the action functional via a mechanism that resembles the vanishing of curl terms in the response function $\langle v'v \rangle$ (for details, see Ref. [37]). Taking together, calculation of the field $\mathbf{B}$ together with the possible restrictions on A are clearly feasible in the full problem. However, the corresponding calculations are demanding even in the one-loop order [37] and are in the scope of an ongoing research.

Returning now to the simplified kinematic model of this paper, we note that neglecting the Lorentz-type force term represents actually a useful framework for calculation of beta functions and their corresponding fixed points (including the nature of their stability). The reason lies in the fact that the analysis of above quantities in the present model and in the full model with incorporated $\mathbf{b}'(\mathbf{b}\partial)\mathbf{b}$ term in the action functional remains actually the same as shown in detail in Ref. [36]. Moreover, in the limiting case of $A = 1$ beta functions, fixed points and their stability do not differ at all. The difference, however lies in that fact that in the full model additional divergences are generated by $\mathbf{b}'(\mathbf{b}\partial)\mathbf{b}$ term of the action functional. Removal of such divergences requires the fields $\mathbf{b}$ and $\mathbf{b}'$ to be renormalized. This means that new anomalous exponents associated to the fields emerge. Subsequently, one requires these for the correct calculation of large-scale asymptotic behavior of the response and correlation functions. However, according to Ref. [36], they actually have no impact on the form of beta functions nor do they change the fixed points and their stability in the present kinematic model. This feature is clearly maintained even for arbitrary values of A.

We further stress that in this paper we are interested in the values of the effective inverse turbulent Prandtl number u_{eff} given according to the definitions of Ref. [15] where it is given as the ratio of the response functions $\langle v'v \rangle$ and $\langle b'b \rangle$ (for details, see also Sec. V of this paper). Since the fields $\mathbf{b}'$ and $\mathbf{b}$ in the full model do get renormalized it may appear that the behavior of the response function $\mathbf{b}'$ may be significantly altered within the full model. However, the sum of anomalous exponents corresponding to fields $\mathbf{b}'$ and $\mathbf{b}$ vanishes which means that asymptotic behavior of the response function $\langle b'b \rangle$ is not altered and remains the same even after inclusion of the Lorentz-type terms within the full model. Thus, the effective turbulent Prandtl number calculated here remains unaffected.

Thereby, we shall leave the problem of the linear divergences untouched in this paper and concentrate only on the problem of the existence and stability of the IR scaling regime, which can be studied without considering the linear divergences discussed above. Bearing the problem of linear ρ divergences in mind, we write the renormalized action functional as

$$\begin{aligned} S(\Phi) = {} & \frac{1}{2} \int dt_1\, d^d\mathbf{x}_1\, dt_2\, d^d\mathbf{x}_2 \\ & \times \left[v'_i(x_1) D^v_{ij}(x_1;x_2) v'_j(x_2) + b'_i(x_1) D^b_{ij}(x_1;x_2) b'_j(x_2) \right] \\ & + \int dt\, d^d\mathbf{x} \{ \mathbf{v}'[-\partial_t + \nu Z_1 \triangle - (\mathbf{v}\cdot\partial)]\mathbf{v} \\ & + \mathbf{b}'[-\partial_t \mathbf{b} + \nu u Z_2 \triangle \mathbf{b} - (\mathbf{v}\cdot\partial)\mathbf{b} + A(\mathbf{b}\cdot\partial)\mathbf{v}] \}, \end{aligned} \tag{13}$$

with Z_1 and Z_2 being the renormalization constants connected with the previously defined renormalization constants $Z_i = Z_i(g,u;d,\rho;\varepsilon)$ with $i \in \nu, g, \mu$ via the equations

$$Z_\nu = Z_1, \quad Z_g = Z_1^{-3}, \quad Z_u = Z_2 Z_1^{-1}. \tag{14}$$

Each of the renormalization constants Z_1 and Z_2 corresponds to a different class of Feynman diagrams (as discussed below) but they share an analogous structure within the MS scheme: the nth order of perturbation theory corresponds to the nth power of g with the corresponding expansion coefficient containing a pole in ε of multiplicity n and less, i.e.,

$$Z_1(g;d,\rho;\varepsilon) = 1 + \sum_{n=1}^{\infty} g^n \sum_{j=1}^{n} \frac{z^{(1)}_{nj}(d,\rho)}{\varepsilon^j}, \tag{15}$$

$$Z_2(g,u;d,\rho;\varepsilon) = 1 + \sum_{n=1}^{\infty} g^n \sum_{j=1}^{n} \frac{z^{(2)}_{nj}(u,d,\rho)}{\varepsilon^j}, \tag{16}$$

where $z^{(1)}_{nj}(d,\rho)$ and $z^{(2)}_{nj}(u,d,\rho)$ are free of the parameter ε. Using the last expressions with renormalized variables inserted

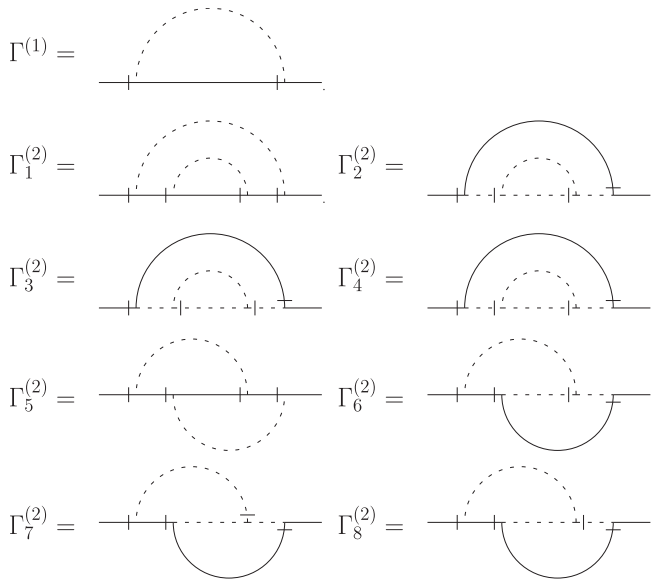

FIG. 3. One-loop and two-loop diagrams that contribute to the self-energy operator $\Sigma^{b'b}(\omega,p)$ in Eq. (18).

leads to divergence free 1-irreducible Green's functions $\langle v_i' v_j\rangle_{1-ir}$ and $\langle b_i' b_j\rangle_{1-ir}$. Moreover, 1-irreducible Green's functions $\langle v_i' v_j\rangle_{1-ir}$ and $\langle b_i' b_j\rangle_{1-ir}$ are associated with the corresponding self-energy operators $\Sigma^{v'v}$ and $\Sigma^{b'b}$ by the Dyson equations which in the frequency-momentum representation read as

$$\langle v_i' v_j\rangle_{1-ir} = [i\omega - \nu_0 p^2 + \Sigma^{v'v}(\omega,\mathbf{p})]P_{ij}(\mathbf{p}), \quad (17)$$

$$\langle b_i' b_j\rangle_{1-ir} = [i\omega - \nu_0 u_0 p^2 + \Sigma^{b'b}(\omega,\mathbf{p})]P_{ij}(\mathbf{p}). \quad (18)$$

Thus, substitution of $e_0 = e\mu^{d_e} Z_e$ for $e = \{g,u,v\}$ is required to lead to UV convergent equations (17) and (18) which in turn determine the renormalization constants Z_1 and Z_2 up to an UV finite contribution. The employed MS scheme fixes then the renormalization constants in the form of $1 + poles\ in\ \varepsilon$ and the coefficients $z_{nj}^{(i)}$, $i = 1,2$ are then fully prescribed in the corresponding order of perturbation theory (see Fig. 3).

The aim of this paper consists of deriving the two-loop perturbative results for the A model with helical effects included via proper definition of Eq. (4). Since in the limit $\rho \to 0$ the less general nonhelical model of Ref. [14] is recovered, all nonhelical results of Ref. [14] have to be reproduced here. Moreover, all quantities depending exclusively on velocity field $\mathbf{v}$ follow only from stochastic Navier-Stokes equation (2) and the correlator (4). In Refs. [11,26], exactly the same conditions were imposed on the velocity type of the fields $\mathbf{v}$ and $\mathbf{v}'$ in the two-loop calculations of the given model. Consequently, the corresponding quantities depending exclusively on the velocity type of fields in the present model have to equal those obtained in Refs. [11,26]. Taking together, Z_1 in the present model must be the same as in Ref. [26] while nonhelical values of Z_2 in the generalized helical A model must reproduce results of Ref. [14]. Thus, before generalizing the approach of Refs. [14,15] to the more general A model with helical contributions, we review results of Refs. [11,14,15] which are relevant for this paper.

Let us start with the coefficients related to $\mathbf{v}$ and $\mathbf{v}'$ which comprise the renormalization coefficient Z_1. As stated above, the present model and the model under study in Refs. [11,26] have the same renormalization constant Z_1 and the expansion coefficient $z_{11}^{(1)}$ is therefore given as

$$z_{11}^{(1)} = -\frac{S_d}{(2\pi)^d}\frac{(d-1)}{8(d+2)}, \quad (19)$$

where S_d is the surface area of the d-dimensional unit sphere defined as $S_d \equiv 2\pi^{d/2}/\Gamma(d/2)$ with $\Gamma(x)$ being the standard Euler gamma function. Thus, no helical contributions at the one-loop level emerge for quantities involving only the velocity type of the fields $\mathbf{v}$ and $\mathbf{v}'$. In Ref. [26], the two-loop order coefficient $z_{22}^{(1)}$ is shown to satisfy

$$z_{22}^{(1)} = -\left(z_{11}^{(1)}\right)^2. \quad (20)$$

Consequently, $z_{22}^{(1)}$ is also ρ independent and only the remaining coefficient $z_{21}^{(1)}$ contains helical contributions to Z_1. Since the corresponding expression from Ref. [11] is rather huge, we shall not reprint it here.

Let us now turn our attention to Z_2 which requires to analyze the structure of the self-energy operator $\Sigma^{b'b}$ in the Dyson equation (18). In the two-loop order, $\Sigma^{b'b}$ equals the sum of singular parts of nine 1-irreducible Feynman diagrams as shown in Fig. 3. Using the notation of Ref. [14] for the sake of easier comparison, we write the two-loop approximation of $\Sigma^{b'b}$ as

$$\Sigma^{b'b} = \Gamma^{(1)} + \Gamma^{(2)} = \Gamma^{(1)} + \sum_{l=1}^{8} s_l \Gamma_l^{(2)}, \quad (21)$$

where $\Gamma^{(1)}$ represents the single one-loop diagram shown in Fig. 3 and $\Gamma^{(2)}$ represents the sum of the eight two-loop diagrams shown in Fig. 3. The terms s_l, $l = 1,\ldots,8$, denote the corresponding symmetry factors which equal 1 for all diagrams except for the fourth with $s_4 = \frac{1}{2}$.

The single one-loop diagram of Fig. 3 apparently does not include the propagator $\langle v_i v_j\rangle_0$ which is the only diagrammatic object that contains helical contributions. The corresponding coefficient $z_{11}^{(2)}$ that follows from the $\Gamma^{(1)}$ contribution is thus actually also ρ independent. Since all nonhelical quantities in the present helical A model must reproduce the corresponding values of Ref. [14], the following $z_{11}^{(2)}$ expansion coefficient must be obtained (as verified also by direct calculation):

$$z_{11}^{(2)} = -\frac{S_d}{(2\pi)^d} \times \frac{(d^2-3)(u+1) + A[d+u(d-2)] + A^2(1+3u)}{4d(d+2)u(u+1)^2}. \quad (22)$$

The contributions to $\Gamma^{(2)}$ which determine $z_{22}^{(2)}(d,\rho)$ and $z_{21}^{(2)}(d,\rho)$ are given by the eight two-loop diagrams of Fig. 3. After a quick inspection we notice that each of the diagrams contains two $\langle v_i v_j\rangle_0$ propagators which are linearly dependent on the helicity parameter ρ. Thus, all two-loop diagrams can depend only quadratically on ρ (linear dependencies are not relevant for the present calculations and are dropped systematically). Thus, using the notation equivalent to that of Ref. [14] we can write the divergent part of $\Gamma^{(2)}$ in the

following form:

$$\Gamma^{(2)} = \frac{g^2 \nu\, p^2\, S_d}{16(2\pi)^{2d}} \left(\frac{\mu}{m}\right)^{4\varepsilon} \frac{1}{\varepsilon} \left\{ \frac{S_d}{\varepsilon} C^\rho + B^{(0)} + \rho^2 \delta_{3d} B^{(\rho)} \right\}, \tag{23}$$

where C^ρ, $B^{(0)}$, and $B^{(\rho)}$ are for now undetermined. The d,g,p,μ,u,m dependent factors in Eq. (23) could principally by absorbed into C^ρ, $B^{(0)}$, and $B^{(\rho)}$, but are kept in order to comply with notation of Ref. [14]. By definition, $B^{(0)}$ encodes nonhelical contributions of the corresponding diagrams and for $\rho \to 0$ must yield the same expressions as shown in Ref. [14]. Since $B^{(0)}$ was not explicitly introduced in Ref. [14] we define it via

$$B^{(0)} = S_{d-1} \int_0^1 dx\ (1-x^2)^{(d-1)/2}\ B, \tag{24}$$

where the variable x denotes the cosine of the angle between two independent loop momenta $\mathbf{k}$ and $\mathbf{q}$ of the two-loop diagrams, i.e., $x = \mathbf{k}\cdot\mathbf{q}/|k|/|q|$. The function B is obtained in the same form as in Ref. [14] but is rather huge and shall not be reproduced here. We merely notice that within the scope of the present calculations we have determined $B^{(0)}$ directly by the methods discussed later in connection with the helical contributions in the present model. Furthermore, the expression C^ρ is directly related to the second order pole coefficient of Z_2, namely, to $z_{11}^{(2)}(d,\rho)$. Although we denoted this contribution by superscript ρ, in reality it must be independent of helical contributions because of the one-loop order of the present generalized A model which is completely free of any helical effects. Consequently, second order ε pole contributions to $\Gamma^{(2)}$ have to remain also ρ independent and the superscript ρ in C^ρ may be dropped, i.e., $C^\rho \equiv C$. Due to helical independence of C it assumes the same form as in Ref. [14] yielding thus the corresponding $z_{22}^{(2)}(d,\rho)$ as

$$z_{22}^{(2)}(d,\rho) = z_{22}^{(2)}(d) = -\frac{S_d^2}{(2\pi)^{2d}} \frac{C}{16u}. \tag{25}$$

At this place, we only briefly note that C is a polynomial of fourth order in A and postpone the details to later on. Equations (19)–(25) thus briefly summarize the results common to the present model and the models of Refs. [11,14,15]. Passing to our generalized helical A model requires now an explicit calculation of helical contributions to $\Gamma^{(2)}$. We once again stress that although $B^{(\rho)}$ is calculated with the explicit d dependence, the helical contributions make sense only for $d = 3$ as indicated by the insertion of the Kronecker delta δ_{d3} into Eq. (23).

Before going further, let us now explain the general character of the A dependencies in the expressions $C^\rho \equiv C$, $B^{(0)}$, and $B^{(\rho)}$ without considering the details of the corresponding calculations. According to Fig. 3 and Eqs. (21) and (23), all of the discussed expressions are given by the diagrams $\Gamma^{(1)}$ or $\Gamma_l^{(2)}$ with $l = 1,\ldots,8$. Noting now that the parameter A appears only in the V_{ijl} type vertex as a linear function, we may gain direct insights into the structure of the A dependencies of the given diagrams. To this end, imagine a diagram with only two vertices of the V_{ijl} type. Since each of the vertices contains only a linear function of A when necessary summations on dummy field indices are performed, we get an overall dependence which may include the most a quadratical term in A as a result of two linear terms in A being multiplied together. In other words, the resulting diagram may therefore be only a polynomial in A of order 2 the most. The same reasoning extends also to the case when four V_{ijl} type vertices appear simultaneously in given diagram. Here, the resulting polynomial must be of an order of 4 in A. Of course, since V_{ijl} type vertices are of tensorial nature, summation over field indices in a given diagram may lower the actual order of the polynomials in A while some polynomial coefficients may also vanish completely. However, under any circumstances higher powers of A may not emerge in the graphs. The diagrams Γ_l with $l = 1,\ldots,8$ contain two or four V_{ijl} type vertices and their sum $\Gamma^{(2)}$ must consequently be a polynomial in A of an order of 4 the most. Additionally, $C^\rho \equiv C$ is proportional to the second order pole in ε of $\Gamma^{(2)}$ and must therefore also be a polynomial of an order of 4 the most. The parameters $B^{(0)}$ and $B^{(\rho)}$ are proportional to the corresponding parts of $\Gamma^{(2)}$ and are therefore polynomials in A with order of 4 the most.

Although the previous discussions determine the structure of the diagrams, only a direct calculation may give us the needed coefficients of the resulting polynomials in A. Thus, we have to perform the calculation of the coefficients $z_{21}^{(2)}(u,d,\rho)$ and $z_{22}^{(2)}(d,\rho)$ directly. On the other hand, since all helical properties of the generalized helical A model are encoded by the term $B^{(\rho)}$ and linear ρ divergences are left out in the present model, we note that $z_{21}^{(2)}(u,d,\rho)$ contains a quadratic term in ρ as the only ρ dependent part. However, to correctly determine the exact term proportional to ρ^2, we are required to calculate $B^{(\rho)}$. For this purpose, we use the Dyson equation (18), the relation (21), and the structure of $\Gamma^{(2)}$, as given by Eq. (23). Finally, $z_{21}^{(2)}(u,d,\rho)$ is found as (once again notation of Ref. [14] is used)

$$z_{21}^{(2)}(u,d,\rho) = \frac{S_d}{16u(2\pi)^{2d}} \left(B^{(0)} + \rho^2 \delta_{d3} B^{(\rho)}\right), \tag{26}$$

where $B^{(0)}$ and $B^{(\rho)}$ are defined via Eqs. (23) and (24), respectively. According to Eq. (26), $B^{(\rho)}$ is given by the two-loop diagrams of Fig. 3 and is written in close analogy with Eq. (24) in the following form:

$$B^{(\rho)} = S_{d-1} \int_0^1 dx\ (1-x^2)^{(d-1)/2} \sum_{l=1}^{8} s_l B_l^{(\rho)} \tag{27}$$

and thus define $B_l^{(\rho)}$ as the corresponding helical parts of the $\Gamma_l^{(2)}$ diagrams. Thus, as already discussed, when the limit $\rho \to 0$ is imposed on Eq. (26), the resulting value gives the $B^{(0)}$ coefficient which in turn complies with its corresponding counterpart of Ref. [14]. On the other hand, for $\rho \neq 0$ the eight two-loop graphs contain nonzero terms which via $B^{(\rho)}$ encode all of the helical effects investigated here. In other words, the result of Ref. [14] is only a special case of the present calculations when appropriate limits are taken while for $0 < |\rho| \leqslant 1$ the corresponding expressions are completely unknown and require to be calculated here. For this purpose, for the diagrams $\Gamma_l^{(2)}$, with $l = 2,\ldots,8$, we utilize the derivative technique outlined in Ref. [15] whose prerequisites are fulfilled for selected diagrams with $l = 2,\ldots,8$. However,

in the case of diagram $\Gamma_1^{(2)}$, only its nonhelical value, a special case of the model considered here, can by evaluated using the derivative technique of Ref. [15]. Therefore, the well established techniques outlined, for example, in Ref. [9] are used for the graph $\Gamma_1^{(2)}$. Nevertheless, calculations for all graphs are quite straightforward; however, they result in complicated lengthy expressions and we present them in the Appendix of this paper.

In the end, we have to reexamine the influence of helicity on the properties of the IR scaling regime and its stability. First, since the fields $\mathbf{v}$, $\mathbf{v}'$, $\mathbf{b}$, and $\mathbf{b}'$ are not renormalized, the following simple relation holds:

$$W^R(g,u,\nu,\mu,\dots) = W(g_0,u_0,\nu_0,\dots). \tag{28}$$

It states that the renormalized connected correlation functions $W^R = \langle\Phi\dots\Phi\rangle^R$ differ from their unrenormalized counterparts $W = \langle\Phi\dots\Phi\rangle$ only by the choice of variables (renormalized or unrenormalized) and in the corresponding perturbation expansion (in g or g_0), where the dots stand for arguments untouched by the renormalization [9,10,46]. This means that unrenormalized correlation functions are independent of the scale-setting parameter μ of dimensional regularization. Thus, applying the differential operator $\mu\partial_\mu$ at fixed unrenormalized parameters on both sides of Eq. (28) gives the basic differential RG equation of the following form [9,10]:

$$[\mu\partial_\mu + \beta_g\partial_g + \beta_u\partial_u - \gamma_\nu\nu\partial_\nu]W^R(g,u,\nu,\mu,\dots) = 0, \tag{29}$$

where the so-called RG functions (the β and γ functions) are given as follows:

$$\beta_g \equiv \mu\partial_\mu g = g(-2\varepsilon + 3\gamma_1), \tag{30}$$

$$\beta_u \equiv \mu\partial_\mu u = u(\gamma_1 - \gamma_2), \tag{31}$$

$$\gamma_i \equiv \mu\partial_\mu \ln Z_i, \quad i = 1,2 \tag{32}$$

and are based on relations among the renormalization constants (14) together with the explicit expressions of Z_1 and Z_2 given by (15) and (16), respectively. To obtain the IR asymptotic behavior of the correlation functions deep inside of the inertial interval, we need to identify the coordinates (g_*, u_*) of the corresponding IR stable fixed point where β_g and β_u vanish, i.e.,

$$\beta_g(g_*) = 0, \quad \beta_u(g_*,u_*) = 0, \tag{33}$$

where $g_* \neq 0$ and $u_* \neq 0$ in the two-loop approximation are required to have the form

$$g_* = g_*^{(1)}\varepsilon + g_*^{(2)}\varepsilon^2 + O(\varepsilon^3), \tag{34}$$

$$u_* = u_*^{(1)} + u_*^{(2)}\varepsilon + O(\varepsilon^2). \tag{35}$$

It may be verified by a direct calculation that at nontrivial fixed points, the following expressions hold:

$$g_*^{(1)} = \frac{(2\pi)^d}{S_d}\frac{8(d+2)}{3(d-1)}, \tag{36}$$

$$g_*^{(2)} = \frac{(2\pi)^d}{S_d}\frac{8(d+2)}{3(d-1)}\lambda, \tag{37}$$

$$u_*^{(1)} = \frac{1}{3a_2}\left(-2a_2 - \frac{\sqrt[3]{2}b_1}{\sqrt[3]{b_2+b_3}} + \frac{\sqrt[3]{b_2+b_3}}{\sqrt[3]{2}}\right), \tag{38}$$

$$u_*^{(2)} = \frac{2(d+2)}{d[1+2u_*^{(1)}]}\left[\lambda - \frac{128(d+2)^2}{3(d-1)^2}\mathcal{B}(u_*^{(1)})\right], \tag{39}$$

where λ is related to the coefficient $z_{21}^{(1)}$ in Eq. (15) as

$$\lambda = \frac{2}{3}\frac{(2\pi)^{2d}}{S_d^2}\left[\frac{8(d+2)}{d-1}\right]^2 z_{21}^{(1)}. \tag{40}$$

The coefficient $\mathcal{B}(u_*^{(1)})$ will be discussed in the text below. Let us now give the explicit expressions for a_i with $i \in 0,1,2$ and b_i with $i \in 1,2,3$. They read as

$$b_1 = a_2(3a_1 - 4a_2), \tag{41}$$

$$b_2 = a_2^2(-27a_0 + 18a_1 - 16a_2), \tag{42}$$

$$b_3 = \sqrt{4b_1^3 + b_2^2}, \tag{43}$$

$$a_0 = -2[d^2 - 3 + A(A+d)], \tag{44}$$

$$a_1 = 6(1-A^2) - 2A(d-2) - d(d+1), \tag{45}$$

$$a_2 = d(d-1). \tag{46}$$

The value of the coefficient a_1 differs from that presented in Ref. [14] where most probably a typesetting error occurred since for $\rho \to 0$ our present result reproduces the less general nonhelical model of Ref. [14]. Moreover, a_1 from Ref. [14] takes the same form as the current one when the (probably misplaced) brackets are corrected.

As already mentioned, one-loop results given by Eqs. (36) and (38) are free of helical contributions (see Fig. 4). Furthermore, $g_*^{(2)}$ depends exclusively on the properties of the underlying velocity field which means that it is common within a class of models with passively advected admixtures, as discussed, for example, in Ref. [11]. In more detail, $g_*^{(2)}$ is completely determined by λ from Eq. (40). However, $u_*^{(2)}$ is model specific and known only for special choices of $A \in 0,1$ [11]. Here, it is expected to contain helical contributions via the quantity $\mathcal{B}(u_*^{(1)})$ which in turn is completely given by the coefficient $z_{21}^{(2)}$ in Eq. (26) and it obtains the following value at

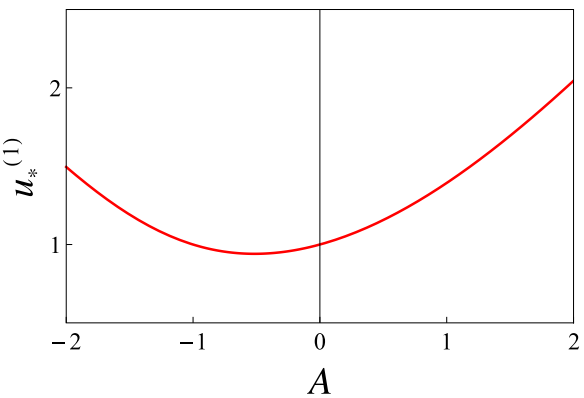

FIG. 4. Dependence of the one-loop inverse turbulent Prandtl number $u_*^{(1)}$ on the parameter A in the region $-2 \leqslant A \leqslant 2$. Note that for $A = -1$ one obtains $u_*^{(1)} = 1$. Apparently, one-loop values of $u_*^{(1)}$ are always positive ($u_*^{(1)} \to \infty$ for $A \to \pm\infty$) and therefore physical for all arbitrary real A.

$u = u_*^{(1)}$:

$$\mathcal{B}(u_*^{(1)},\rho) = \frac{(2\pi)^{2d}}{S_d^2} z_{21}^{(2)}(u_*^{(1)},\rho). \tag{47}$$

We retained the d dependencies for notation purpose. However, only spatial dimension $d = 3$ is physically meaningful when helical effects are considered. The IR behavior of the fixed point is determined by the matrix of the first derivatives which is given as

$$\Omega_{ij} = \begin{pmatrix} \partial\beta_g/\partial g & \partial\beta_g/\partial u \\ \partial\beta_u/\partial g & \partial\beta_u/\partial u \end{pmatrix} \tag{48}$$

and is evaluated for given (g_*, u_*). The present matrix is triangular since β_g is independent of u. Consequently, $\partial\beta_g/\partial u = 0$ and diagonal elements $\partial\beta_g/\partial g$ and $\partial\beta_u/\partial u$ correspond directly to the eigenvalues of the present matrix. Using numerical analysis one can show that the real parts of the diagonal elements are positive for all values of A in the vicinity of $\epsilon = 0$. Furthermore, we have also shown that including spatial parity violation shifts the values of the present matrix even further to positive values. In the end, we stress the well-known fact that β functions of the present model are exactly given even at the one-loop order since all higher order terms cancel mutually, which means that the anomalous dimensions $\gamma_1^* = \gamma_2^*$ equal exactly $2\varepsilon/3$ at the IR stable fixed point.

V. HELICITY AND THE TURBULENT PRANDTL NUMBER

As discussed in the text above, all one-loop contributions to the renormalization constants Z_1 and Z_2 are free of helical contributions even when turbulent environments with broken spatial parity are considered explicitly [14,15]. In the previous section, we have therefore determined the two-loop values of the renormalization constants Z_1 and Z_2 which in fact do manifest helical effects for both renormalization constants. Additionally, a stable nontrivial IR fixed point is shown to exist for the given g^* and u^* in the two-loop order of calculation. Therefore, one may expect that the two-loop order is sufficient to capture the leading order helical contributions to the required turbulent Prandtl number which then of course correspond to the two-loop order of the given perturbative theory. We prove this assertion in the subsequent text by explicit determination of the corresponding values of the turbulent Prandtl number for a range of values of the continuous parameter A. However, we show explicitly that some regions of A have to be omitted when spatial parity violation is weak enough.

The two-loop calculation presented here is analogous to that of Ref. [15]. In this respect, we would therefore like to stress that the turbulent Prandtl number here is the so-called effective turbulent Prandtl number and its calculation is based on the singularities of the corresponding response functions [for the details, see Eq. (11) of Ref. [15]]. Moreover, due to the passive nature of the admixtures considered here and in Refs. [11,14,15], we note that all present quantities independent of the admixture field **b** have to be identical to those of Refs. [11,14,15]. Therefore, the helical properties specific for the given admixture type described by Eq. (1) are in the two-loop order of perturbation theory of the corresponding field theoretic model completely encoded by the two-loop Feynman graphs of Fig. 3.

Taking together, although the present calculations are analogous to those of Refs. [11,15], all quantities connected with the given admixtures and their interactions have to be reexamined here. We also stress that formula (33) of Ref. [15] holds inside of the inertial interval and does not depend on the renormalization scheme. The details of the calculations are outlined in Ref. [15] and we omit them here. The resulting two-loop expression for the inverse turbulent Prandtl number is obtained as

$$u_{\text{eff}} = u_*^{(1)}\Bigg(1 + \varepsilon\Bigg\{\frac{1+u_*^{(1)}}{1+2u_*^{(1)}}\Bigg[\lambda - \frac{128(d+2)^2}{3(d-1)^2}\mathcal{B}(u_*^{(1)})\Bigg] + \frac{(2\pi)^d}{S_d}\frac{8(d+2)}{3(d-1)}[a_v - a_b(u_*^{(1)})]\Bigg\}\Bigg), \tag{49}$$

where ε and the dimension d are taken to their physical values of $\varepsilon = 2$ and $d = 3$, the one-loop value of the inverse turbulent Prandtl number $u_*^{(1)}$ is given in Eq. (38), $\mathcal{B}(u_*^{(1)})$ is defined in Eq. (47), and λ is shown in Eq. (40). The following numerical value corresponds to λ in $d = 3$ as considered here for helical environments:

$$\lambda = -1.0994 \tag{50}$$

which is the same as in Ref. [11] because λ is independent of the admixture type for the passive advection. The remaining parameters a_v and a_b which enter into Eq. (49) are discussed in the text below. Let us first notice that a_v and a_b represent the finite parts of one-loop diagrams with two external velocity type fields $\mathbf{v}, \mathbf{v}'$ and two admixture type fields $\mathbf{b}, \mathbf{b}'$, respectively. Since turbulent velocity environments here and in Ref. [15] are the same, the coefficient a_v must also be the same and we shall not reproduce its analytic form here. In $d = 3$, it can however be easily evaluated numerically as

$$a_v = -0.047718/(2\pi^2). \tag{51}$$

Contrary, a_b is model specific and is given by the finite part of one-loop 1-irreducible diagram $\Gamma^{(1)}$ making it also ρ independent. As already discussed, the present generalized helical A model and the less general model introduced in Ref. [14] have all one-loop quantities, including a_b, identical due to helical effects being pronounced first in the two-loop order. Since a_b plays a crucial role in the two-loop calculation of the inverse turbulent Prandtl number, we show it explicitly in this paper. After straightforward calculation discussed, for example, in Ref. [15], one obtains a_b in the same form as the authors of Ref. [14]. It reads as

$$a_b(u) = -\frac{S_{d-1}}{2u(d-1)(2\pi)^d}\int_0^\infty dk \int_{-1}^1 dx\,(1-x^2)^{\frac{d-1}{2}}\Bigg(\frac{k\{k^3xA(1-A) + k^2[x^2(1-A^2) + A + d - 2] + 2kx(d-1) + d - 1\}}{(k^2+2kx+1)[(1+u)k^2 + 2ukx + u]} - \frac{\Theta(k-1)\{kA(1-A)(1+u)x + A^2(1+3u)x^2 + A[1+u-2(1+2u)x^2] + (1+u)(x^2+d-2)\}}{k(1+u)^2}\Bigg) \tag{52}$$

TABLE I. Numerical values of $u^{(0)}(A)$ and $u^{(\rho)}(A)$ for selected values of A which are required to obtain the turbulent Prandtl number defined as $\mathrm{Pr}_A = 1/[u^{(0)}(A) + \rho^2 u^{(\rho)}(A)]$. Values at $A = -2$, 2.5, and 3 demonstrate physical constraints $-1.723 < A < 2.800$ required for present calculations to be meaningful for all values of ρ.

A	-2	-1.5	-1.0	-0.5	0	$+0.5$	$+1.0$	$+1.5$	$+2.0$	$+2.5$	$+3.0$
$u^{(0)}(A)$	-0.4663	$+0.3726$	$+1.000$	$+1.2705$	$+1.3685$	$+1.4436$	$+1.4205$	$+1.2145$	$+0.8343$	$+0.3339$	-0.2355
$u^{(\rho)}(A)$	$+1.0503$	-0.0163	-0.000	$+0.3587$	$+0.2376$	-0.0854	$+0.0623$	$+0.9444$	$+2.4408$	$+4.3269$	$+6.4228$

with Θ being the usual Heaviside step function. One further difference to Ref. [15] is manifested even at the one-loop order in the already calculated value of $u_*^{(1)}$. Due to the tensorial interaction structures in the present model, it obtains the form of Eq. (38) which is of course different from the corresponding value obtained in Ref. [15]. Using expression (49) with all necessary coefficients now known due to Eqs. (38), (40), (47), (51), and (52), we may proceed to the actual calculation of the Prandtl number. As already discussed, using the RG techniques in theory of critical behavior requires to substitute $\varepsilon = 2$ in the final expressions as thoroughly discussed, for example, in Refs. [4,9]. The spatial dimension is set to $d = 3$, as required by the nature of the helical problem. Inserting all necessary quantities into Eq. (49) we obtain its values for arbitrary A and get the inverse turbulent Prandtl number u_{eff} as a function of A as indicated explicitly by denoting the corresponding values as $u_{\mathrm{eff}}(A)$.

The corresponding Eqs. (49), (38), (40), (47), (51), and (52) are all known in analytic form. Nevertheless, due to the complicated analytic structure of the coefficient $z_{12}^{(2)}$, the expression in Eq. (47) is a complicated analytic function of model variables. Thus, the resulting analytic expression for the inverse turbulent Prandtl number is complicated too and we shall present it in the Appendix of this paper. However, for further discussion it is convenient to split $u_{\mathrm{eff}}(A)$ into its nonhelical part $u^{(0)}(A)$ and its corresponding helical contribution $\rho^2 u^{(\rho)}(A)$ via

$$u_{\mathrm{eff}}(A) = u^{(0)}(A) + \rho^2 u^{(\rho)}(A). \tag{53}$$

Note that both $u^{(0)}(A)$ and $u^{(\rho)}(A)$ are defined to be independent of ρ. Nevertheless, $u^{(\rho)}(A)$ stands in front of the helical contribution in Eq. (53) and thus encodes all helical effects of the present model. Both $u^{(0)}(A)$ and $u^{(\rho)}(A)$ are complicated analytic functions of model parameters and we shall present them here only via their graphical representation given in Fig. 5, which is sufficient for the interpretation of the obtained results. Moreover, for a few selected values of parameter A the corresponding numerical values are given in Table I. In Fig. 5, we plot $u^{(0)}(A)$ in the region of $-2 \leqslant A \leqslant 3$ as it contains all zero points of the present function. Due to the same reasoning, $u^{(\rho)}(A)$ is plotted in a smaller region of $-2 \leqslant A \leqslant 2$. The actual turbulent Prandtl number Pr_A is then given as the inverse of $u_{\mathrm{eff}}(A)$. Explicitly,

$$\mathrm{Pr}_A = \frac{1}{u^{(0)}(A) + \rho^2 u^{(\rho)}(A)}. \tag{54}$$

However, in the immediately following text we shall rather use the corresponding values of the inverse turbulent Prandtl number as they better suit our next discussion. Afterwards, we discuss the turbulent Prandtl numbers in the helical A model for selected values of A.

Considering first the nonhelical part $u^{(0)}(A)$ of the inverse turbulent Prandtl, we note that contrary to Ref. [14] our analysis was not limited to the interval $-1 \leqslant A \leqslant 1$ and included the more general helical case. Nevertheless, our result on $u^{(0)}(A)$ is in complete agreement with the nonhelical model of Ref. [14] for $-1 \leqslant A \leqslant 1$ but shows also additionally the important zero points of the function $u^{(0)}(A)$. This clearly demonstrates that the effective value of the corresponding diffusion coefficient should be infinitesimally small when approaching values of A at the zero points of $u^{(0)}(A)$ located at $A = -1.723$ and 2.800 (numerical values rounded to 3 decimal places). Consequently, by approaching the zero points of $u^{(0)}$, the turbulent Prandtl numbers would obtain infinitely large values. Additionally, according to Fig. 5, the inverse turbulent Prantdl number would obtain unphysical negative values for $A < -1.723$ and $A > 2.800$.

Thus, for nonhelical turbulent environments constraints $-1.723 \leqslant A \leqslant 2.800$ must be imposed on values of A in the the two-loop order of perturbation theory which is a result not obtained by the authors of Ref. [14] due to constraining their analysis to $-1 \leqslant A \leqslant 1$. Additionally, values of A close to zero points of $u^{(0)}(A)$ should also be considered only with extreme caution as the resulting turbulent Prandtl numbers tend to $+\infty$ at the border of the allowed interval. On the other hand, such a problem did not occur for the corresponding one-loop values as clearly demonstrated in Fig. 4 in this paper. It is, therefore, clear that constraints for nonhelical environments arise only in connection with the two-loop order calculation used here and are therefore inherently given by the structure of perturbation theory of the A model. In other words, such constraints are not inherent in values of A outside of the usually

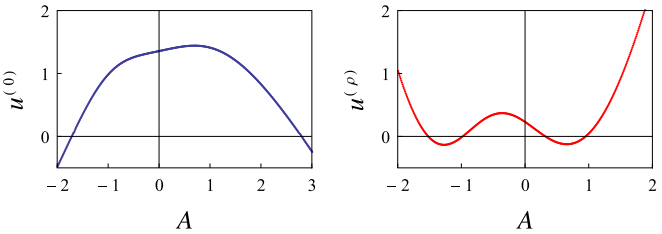

FIG. 5. Dependence of $u^{(0)}$ and $u^{(\rho)}$ on parameter A shown in regions $-2 \leqslant A \leqslant 3$ and $-2 \leqslant A \leqslant 2$, respectively. Quantity $u^{(0)}$ corresponds to nonhelical value of inverse turbulent Prandtl number, while $u^{(\rho)}$ represents helical contribution to the inverse turbulent Prandtl number. Points represent numerical values obtained from Eq. (53).

studied region $-1 \leqslant A \leqslant 1$ and represent only an artifact of the perturbative approach. Such a conclusion is supported also by the special case of $A = -1$ discussed later in more detail. It is also important to state that restrictions on the values of A have already been observed in Ref. [16] where the interval of $-0.581 < A < 0.613$ is identified. Although our interval is larger, there is no contradiction as authors of Ref. [16] investigated the A model of passive advection in the simplified model with the velocity field $\mathbf{v}$ being specified by a Kraichnan ensemble. Moreover, different stability criteria are imposed here as already discussed in Sec. V.

For now on, we stress that all previous conclusions are completely true only in nonhelical environments. Bearing in mind the constraints on A in the nonhelical case, we also notice that $u^{(0)}(A)$ has a maximum at $A = 0.7128$ (rounded on last presented number) and is quite well stable in the range of approximately $-0.5 < A < 1.5$ which in connection with the results on one-loop order values presented, for example, in Fig. 4 also explains the remarkable stability of models with $A = 0$ and 1 against the order of perturbation theory, as already noticed in Ref. [14]. A qualitatively similar picture holds also when helical contributions are considered, as discussed below.

Let us now turn our attention to $u^{(\rho)}$ which encodes the much needed helical contributions of our generalized helical A model. Its graphical representation is given in Fig. 5 and its sign determines the character of helical dependence of $u_{\mathrm{eff}}(A)$. Explicitly, for positive (negative) values of $u^{(\rho)}(A)$ the corresponding inverse turbulent Prandtl number will be a monotonically growing (descending) function of the helicity parameter ρ. The zero points of $u^{(\rho)}(A)$ therefore turn out to represent cases where helical effects have no impact on diffusion-advection processes. Their location is determined numerically based on the previous analysis with the resulting values being -1.516, -1.000, 0.325, and 0.912 (numbers rounded to 3 decimal places).

Furthermore, inserting values of the functions $u^{(0)}(A)$ and $u^{(\rho)}(A)$ into Eq. (49) one may easily calculate the inverse turbulent Prandtl number $u_{\mathrm{eff}}(A)$ as a function of A for selected values of ρ. The resulting values are presented in Fig. 6 and show a highly interesting behavior. In the nonhelical case, the resulting turbulent Prandtl numbers clearly obtain unphysical values in restricted intervals $A < -1.723$ and $A > 2.800$. However, $u^{(\rho)}(A)$ is according to Fig. 5 in both restricted intervals not only positive, but it also evidently satisfies $u^{(\rho)}(A) > |u^{(0)}(A)|$. Therefore, there exists some critical value of the helicity parameter ρ for which the corresponding inverse turbulent Prandtl number $u_{\mathrm{eff}} = u^{(0)} + \rho^2 u^{(\rho)}$ gets positive for all values of A. In other words, when spatial parity violation is strong enough, the resulting inverse turbulent Prandtl number obtains always positive values. Thus, introducing parity violation into the turbulent system improves perturbative series for the present model, as explicitly demonstrated in Fig. 6. In this respect, we notice that increasing ρ from 0 up to $\rho \approx 0.749$ (rounded to 3 decimal places) enlarges the region of physically allowed values of A without any bounds. This is evident from u_{eff} starting to grow (fall) for $A \to +\infty$ ($A \to -\infty$) when the critical value of $\rho \approx 0.749$ is exceeded. Strikingly, it is not required to reach the maximum possible violation of parity ($|\rho| = 1$) to remove the constraints on A.

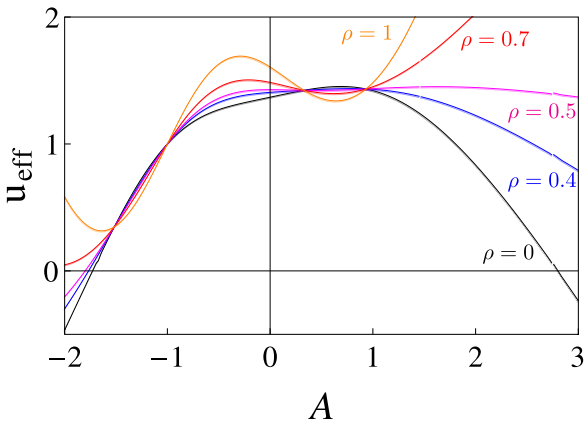

FIG. 6. Inverse turbulent Prandtl number u_{eff} as a function of A shown for fixed values of ρ in the range of $-2 \leqslant A \leqslant 3$. On the right side of the graph, in the region of approximately $A > 1$, the dependencies for selected values of ρ are stacked one above the other with $\rho = 1$ (orange) being on the top while the remaining dependencies follow in the successive order of $\rho = 0.7$ (red), $\rho = 0.5$ (magenta), $\rho = 0.4$ (blue), and $\rho = 0$ (black). Note that for $\rho = 1$ the function is apparently bound from below but unbound from above which is a behavior observed for all $\rho > 0.749$ which represents a threshold value of helicity above which the stationary regimes of the system are fully stabilized.

Contrary, by exceeding the critical value of $\rho = 0.749$ we remove any constraints on A completely. In other words, beyond the critical value of $\rho = 0.749$ all inverse turbulent Prandtl numbers are positive and thus physical. Consequently, exceeding the threshold of $\rho = 0.749$ stabilizes the diffusion-advection processes in the general A model to a large extent. This clearly means that helicity has an extensive stabilizing effect on stationary regimes in the present model, which resembles the results obtained previously in Refs. [51–53], where specific models of fully developed turbulence were analyzed based on the principle of maximal randomness. Here, the authors showed that stabilization occurs near to the maximal possible value of the helicity parameter. Calculations within the two-loop order of the corresponding perturbative theory are therefore well defined which further supports our hypothesis regarding the artificiality of constraints imposed on values of A in nonhelical environments. The interplay between the interaction parameter A and the parameter ρ describing the amount of spatial parity violation shows thus highly nontrivial behavior.

Additionally, in Fig. 6 we may identify values of A for which the helical dependence of the inverse turbulent Prandtl number is relatively small. Such regions are all connected with the regions of negative values of $u^{(\rho)}$ as seen from Fig. 5 and correspond therefore to the union of interval $-1.516 \leqslant A \leqslant -1.000$ with $0.325 \leqslant A \leqslant 0.912$. Interestingly, we notice that two special cases $A = -1$ and 1 either lie directly in such regions ($A = -1$ case) or are located in a close vicinity of these ($A = 1$ case). First, let us discuss the case of linearized helical NS equations with $A = -1$ which up to date have not been investigated for helical environments in any way. According to the performed numerical analysis of Eq. (50), $u^{(\rho)}$ is less than 10^{-8} at $A = -1$ which in the limits of accuracy means that

$u^{(\rho)}$ is actually equivalent to zero and consequently $A = -1$ corresponds directly to the zero point of $u^{(\rho)}(A)$. We point out that this is not just a trivial influence of vanishing of all helical terms in the two-loop diagrams $\Gamma^{(2)}_l$ with $l = 1, \ldots, 8$. In fact, separately each diagram contains the corresponding helical terms which, however, mutually cancel each other when all diagrams are summed up together, as required in deriving of $\Sigma^{b'b}$. As a consequence, at $A = -1$ the properties of the flow are completely independent of spatial parity violation of the underlying fully developed turbulent velocity flow. Moreover, this result is most probably independent of perturbation order as suggested by $u^{(0)}$ being exactly one (within the accuracy of the present numerical analysis) at both the first and the second orders of the corresponding perturbation order. A similar hypothesis has already been stated by the authors of Refs. [14] for nonhelical values. Here, we however demonstrate that such a behavior persists even in helical environments.

In this respect, it is also worth mentioning that for $A = 1.038$ (rounded to 3 decimal places), one- and two-loop values of the nonhelical inverse turbulent Prandtl number do also coincide, a result which was not observed in Ref. [14] due to constraining the analysis only at $-1 \leqslant A \leqslant 1$. However, unlike in the $A = -1$ case, helical effects are present quite significantly for the $A = 1.038$ case (as later discussed more closely, the difference between the nonzero value of the turbulent Prandtl number and its minimal value at $|\rho| = 1$ is around 7%) which means that the model of the linearized Navier-Stokes equations corresponding to the $A = -1$ case in the present model has unique features. The remaining three zero points of $u^{(\rho)}(A)$, i.e., $A \in \{-1.516, 0.325, 0.912\}$, do not show the same behavior. Instead, their one- and the two-loop values differ significantly. Thus, although the remaining three zero points of $u^{(\rho)}(A)$ also lead to models stable against helical effects in the two-loop order, there is no indication that higher order of perturbation theory preserves location of the zero points for the analog of $u^{(\rho)}(A)$ obtained in higher orders.

On the other hand, the equality of the one- and the two-loop results for $A = 1.038$ explains another up to date not well understood result of Ref. [11]. Here, it is observed that the kinematic MHD model corresponding to $A = 1$ of the present model is remarkably stable against one- and two-loop order corrections. Using, however, the previous result, we easily explain this as a consequence of the $A = 1$ case lying in the proximity of $A = 1.038$ where one- and two-loop order values are identical. Such a situation is of course true only in the present two-loop order of the calculation. In higher orders of perturbation theory, the corresponding polynomials over A which occur in the diagrams of Fig. 3 are of higher orders and, consequently, the intersection between higher order analog of $u^{(0)}(A)$ and one-loop order result $u^{(1)}_*$ may dramatically shift to new values. Additionally, contrary to the $A = -1$ case, there is no evidence from helical values that the location of the intersection would be fixed in higher order loop calculations and the relatively small contribution of the two-loop order corrections to the inverse turbulent Prandtl number of the kinematic MHD model should be clearly attributed to the present order of calculations. Additionally, the $A = 1$ case lies close to the value of $A = 0.912$ where the inverse turbulent Prandtl number is independent of any helical effects. Since the function $u^{(\rho)}(A)$ is continuous, it causes the helical effects for all models in the vicinity of the $A = 0.912$ case to be relatively stable against helical effects. The effect manifests itself clearly in the helical values of the corresponding inverse turbulent magnetic Prandtl number of the kinematic MHD model, where the maximum change is less than 5% of its nonhelical value, as already observed but not well explained in Ref. [11].

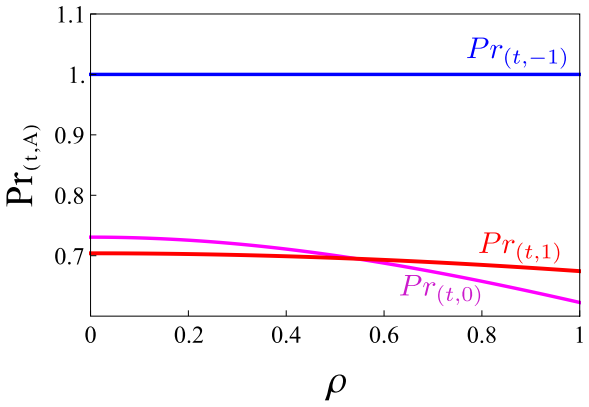

FIG. 7. Helical dependence of the turbulent Prandtl numbers $\mathrm{Pr}_{t,A}$ for three physically important models with $A \in \{-1, 0, 1\}$ shown in the range of $\rho \leqslant 1$. On the top, the dependence for $A = -1$ is shown (blue line). The dependence for $A = 0$ (magenta) is for smaller values of ρ located above the dependence for $A = 1$ (red) which changes around $\rho \approx 0.6$ and pertains up to $\rho = 1$.

Contrary to the special cases discussed above, another physically important model corresponding to the $A = 0$ case lies deep in the interval of positive values of $u^{(\rho)}(A)$ and is thus located far away from the points $A = 0.325$ and 0.912 where $u^{(\rho)}(A)$ has its nearest zero points located. On the other hand, the $A = 0$ model lies relatively closely to the local maximum of the function $u^{(\rho)}(A)$ on the interval of $0.325 \leqslant A \leqslant 0.912$. Consequently, helical effects in the $A = 0$ model are pronounced far greater [almost by a maximum possible amount in the interval of positive values of $u^{(\rho)}(A)$], as seen, for example, by almost 20% change of the inverse turbulent Prandtl number in the helical environments. In other words, function $u^{(\rho)}(A)$ represents an easy tool to assess the importance of helical effects for given values of A in the present model and explains the previously unidentified context between the $A = 0$ and 1 models.

Finally, let us discuss the obtained values of the helical turbulent Prandtl numbers which follow from Eq. (49) and the functions $u^{(0)}$ and $u^{(\rho)}$ which appear therein. For selected parameters A, we show their corresponding numerical values in Table I while their graphical representation is given in Fig. 7 for the three physically important models of $A \in \{-1, 0, 1\}$. As before, the function $u^{(\rho)}(A)$ encodes the behavior of the turbulent Prandtl numbers with respect to ρ for all physically admissible values of A which, as shown before, clearly depend also on the helicity parameter ρ. For the case of the turbulent Prandtl numbers it has, according to Eq. (54), the following meaning: for $u^{(\rho)}(A) > 0$ the turbulent Prandtl number is a decreasing function of ρ, for $u^{(\rho)}(A) < 0$ the turbulent Prandtl

number is an increasing function of ρ and finally for $u^{(\rho)}(A) = 0$ the turbulent Prandtl number is independent of ρ. This means that the turbulent Prandtl numbers do increase with helicity parameter ρ only for values of A satisfying $-1.516 < A < -1$ and $0.325 < A < 0.912$. Excluding the zero points of $u^{(\rho)}(A)$, the remaining values of A lead to monotonically decreasing helical turbulent Prandtl numbers, as already seen in Ref. [11] for the special cases $A = 0$ and 1. While for the $A = 0$ model the helical effects are pronounced more effectively due to the reasons discussed above, the turbulent Prandtl number for the $A = 1$ model corresponding to the kinematic MHD model is less sensitive to helical effects due to its above discussed proximity to the $A = 0.912$ case. We also stress that there are no restrictions on A when the threshold of $\rho \approx 0.749$ is exceeded. Thus, corresponding helical dependencies of the turbulent Prandtl numbers may also be considered for $\rho > 0.749$. Consequently, we see that not the internal vectorial nature of the admixture itself but their interactions with the underlying turbulent field $\mathbf{v}$, as described by the parameter A, are crucial for developing different patterns in regard to helical effects and their influence on diffusion-advection processes. This observation was made even earlier [54,55] but here we established it up to the second order of the perturbation theory.

Summing up, we have shown that the impact of the interactions as given via the parameter value of A has a highly nontrivial impact on diffusion-advection processes when helical environments are considered. The resulting dependencies are truly complicated functions of A and lead to nontrivial effects in connection with the helicity parameter ρ. Therefore, instead of the tensorial nature of the admixture itself we have clearly identified the tensorial structure of interactions to be a more dominant factor which effectively alters the advection-diffusion process in fully developed turbulent environments. Thus, assertions made by the authors of Ref. [11] must partially be revised at least for the case of vector admixtures advected passively in turbulent environments, and a greater than expected impact of interactions on the actual advection-diffusion processes must be recognized. Additionally, we once again stress that present calculations clearly demonstrate that helical effects exert a stabilizing effect on diffusion-advection processes.

VI. CONCLUSION

Using the field theoretic renormalization group technique in the two-loop approximation, we have obtained analytic expressions for the turbulent Prandtl number within the general A model of passively advected vector impurity. Compared to Ref. [14], a more realistic scenario with effects of broken spatial parity has been considered by defining appropriate correlators of stochastic driving forces. Technically, the presence of broken spatial parity is described by the helicity parameter ρ ranging from $|\rho| = 0$ (no parity breaking) to $|\rho| = 1$ (highest possible violation of spatial parity). Since our general helical A model encompasses the less general nonhelical model of Ref. [14] we were able to recover the results of Ref. [14] within the present calculations. However, the parameter a_1, in Eq. (46), was shown to differ from the corresponding nonhelical value of Ref. [14]. However, since all nonhelical results have been confirmed within the scope of our general helical model and only the parameter a_1 is clearly not reproduced, we attribute the difference merely to a typographic error made by the authors of Ref. [14].

Additionally to the helical effects we extended our study of the A model to arbitrary real values of A, as suggested in Ref. [21], whereas in Ref. [14] only the interval $-1 \leqslant A \leqslant 1$ is considered. Nevertheless, although one-loop values of physical quantities have all been shown to obtain meaningful values when passing to the two-loop order we noticed negative values of the turbulent Prandtl numbers for $A < -1.723$ and $A > 2.800$ (numbers rounded to 3 decimal places) in the nonhelical case. Furthermore, we show that the helical effects effectively enhance the stability in the present model and lift the restrictions imposed on A when a critical threshold of $\rho \approx 0.749$ (rounded to 3 decimal places) is exceeded. This points towards the conclusion that restricting A to the interval $-1.723 \leqslant A \leqslant 2.800$ is most probably only an artifact of the two-loop order perturbative calculations. Since in Sec. V we showed that the Feynman diagrams corresponding to the nth order of perturbation theory generally have a form of polynomials in A with the highest possible power of A being $2n$, one may expect that higher orders of loop calculations shift or let all the zero points of the inverse turbulent Prandtl number vanish completely. Such a behavior has already been observed in the one-loop order for the analogous quantity $u_*^{(1)}$. Thus, it would be highly interesting to go beyond the limits of the two-loop order; however, such an analysis is technically demanding and beyond the scope of this paper. Nevertheless, the two-loop order values obtained deep in the interval of $-1.723 \leqslant A \leqslant 2.800$ are well defined which means that the physically most interesting cases of $A \in \{-1,0,1\}$ can be safely considered at least in the two-loop order of perturbation theory. Additionally, the stability of stationary regimes when a critical threshold of $\rho \approx 0.749$ is exceeded resembles helicity effects already observed in the framework of the specific models of developed turbulence [51–53].

For the model of linearized Navier-Stokes equations ($A = -1$) we have obtained helical values of the turbulent Prandtl number equal to 1 regardless of the presence of helical effects. It is therefore natural to expect that also higher orders of perturbation theory preserve the same, a hypothesis already stated by the authors of Ref. [14]. This adds another argument in favor of the hypothesis that problems with range of physically admissible values of A could be resolved completely in higher orders. Physically, the resulting values demonstrate remarkable stability of the $A = -1$ case against helical effects.

Effectively, the $A = 1$ case corresponding to the kinematic MHD model possesses similarities to the $A = -1$ model with regard to its helical properties due to its proximity to the $A = 0.912$ case, where helical effects are not present in the two-loop order. Varying A continuously allowed us to show that high stability of the $A = 1$ model is not due the vectorial nature of the admixture but due to its interactions prescribed by the values of A. Contrary, the $A = 0$ model is shown to lie far from the values of A where the helical effects are not present. Consequently, its turbulent Prandtl number depends significantly on ρ.

Adding together the case of $A = 1$ corresponding to the kinematic MHD turbulence, the case of $A = 0$ model, and the model of linearized Navier-Stokes equations have been brought into the context of a more general A model. The interactions encoded by values of A result in various patterns of behavior of the turbulent Prandtl numbers. Thus, in the regions of $1.516 \leqslant A \leqslant 1.000$ and $0.325 \leqslant A \leqslant 0.912$ (all numbers rounded to 3 decimal places) the corresponding two-loop turbulent Prandtl numbers are monotonically growing with ρ. Moreover, for values of $A \in \{-1.516; -1; 0.325; 0.912\}$ the turbulent Prandtl numbers are independent of ρ but as previously discussed, only the $A = -1$ case is believed to retain this property in higher order loop calculations. Finally, the remaining values of A, which belong to the physically admissible region, possess monotonically decreasing turbulent Prandtl numbers when ρ is increased. We thus conclude that varying the interactions by changing the values of A has a more profound effect on advection-diffusion processes than the tensorial character of the admixture itself, which significantly refines the conclusions made by the authors of Ref. [14].

ACKNOWLEDGMENTS

The work was supported by VEGA Grant No. 1/0223/13 of the Ministry of Education, Science, Research and Sport of the Slovak Republic. The authors gratefully acknowledge the hospitality of the Bogoliubov Laboratory of Theoretical Physics of the Joint Institute for Nuclear Research, Dubna, Russian Federation. P.Z. would like to express his gratitude to M. Dančo for fruitful discussions which helped to carry out investigations presented here.

APPENDIX

Let us now present the results on coefficients $B_l^{(\rho)}$ from Eq. (27) which correspond to helical contributions of graphs $\Gamma_l^{(2)}$ with $l \in 1, \ldots, 8$ shown in Fig. 3. The graphs $\Gamma_l^{(2)}$ with $l \in 2, \ldots, 8$ were calculated using the technique presented in Ref. [15] while the remaining graph $\Gamma_1^{(2)}$ was calculated using the approach described in [9]. In this Appendix, we show explicitly analytic expressions corresponding to the graphs $\Gamma_1^{(2)}$ and $\Gamma_3^{(2)}$ and present the remaining six contributions only graphically as the corresponding analytic expressions are extensive in their length. Let us start now with $B_1^{(\rho)}$. Since it was calculated using a method different to the remaining diagrams, it is more suitable to show not the coefficient B_1^{ρ} but directly its contribution to B^{ρ} with already performed integration over x. Explicitly,

$$\int_0^1 dx (1-x^2)^{\frac{d-1}{2}} B_1^{(\rho)} = 16u(A^2 \tilde{f}^{(2)} + A^3 \tilde{f}^{(3)} + A^4 \tilde{f}^{(4)}), \tag{A1}$$

where A^i with $i \in 2,3,4$ are the corresponding powers of the parameter A while $\tilde{f}^{(i)}$ with $i \in 2,3,4$ are yet unspecified functions labeled by superscripts (i). The terms proportional to A^0 and A^1 vanish, as the corresponding terms cancel each other effectively. They read as

$$\tilde{f}^{(i)} = G_0^{(i)}(d,u) + \sum_{j=1}^{11} g_j^{(i)} G_j(d,u). \tag{A2}$$

Here, $j \in 1, \ldots, 11$ runs over 11 elements of the sum on the right hand side of Eq. (A2). The functions $G_j(d,u)$ carry no index i and are consequently the same for all $i \in 2,3,4$. Contrary, the functions $G_0^{(i)}(d,u)$ and $g_j^{(i)}$ depend on i and shall be discussed later. The functions $G_j(d,u)$ read as

$$G_1(d,u) = {}_2F_1\left[+\frac{1}{2}, +\frac{1}{2}; \frac{d}{2}; \frac{u^2}{(u+1)^2}\right], \tag{A3}$$

$$G_2(d,u) = {}_2F_1\left[-\frac{1}{2}, +\frac{1}{2}; \frac{d}{2}; \frac{u^2}{(u+1)^2}\right], \tag{A4}$$

$$G_3(d,u) = {}_2F_1\left[-\frac{1}{2}, -\frac{1}{2}; \frac{d}{2}; \frac{u^2}{(u+1)^2}\right], \tag{A5}$$

$$G_4(d,u) = {}_2F_1\left[-\frac{3}{2}, -\frac{1}{2}; \frac{d}{2}; \frac{u^2}{(u+1)^2}\right], \tag{A6}$$

$$G_5(d,u) = {}_2F_1\left[-\frac{1}{2}, +\frac{1}{2}; \frac{d+2}{2}; \frac{u^2}{(u+1)^2}\right], \tag{A7}$$

$$G_6(d,u) = {}_2F_1\left[-\frac{1}{2}, +\frac{3}{2}; \frac{d+2}{2}; \frac{u^2}{(u+1)^2}\right], \tag{A8}$$

$$G_7(d,u) = {}_2F_1\left[+\frac{1}{2}, +\frac{1}{2}; \frac{d+2}{2}; \frac{u^2}{(u+1)^2}\right], \tag{A9}$$

$$G_8(d,u) = {}_2F_1\left[+\frac{1}{2}, +\frac{3}{2}; \frac{d+2}{2}; \frac{u^2}{(u+1)^2}\right] \tag{A10}$$

$$G_9(d,u) = {}_2F_1\left[+\frac{1}{2}, +\frac{5}{2}; \frac{d+4}{2}; \frac{u^2}{(u+1)^2}\right], \tag{A11}$$

$$G_{10}(d,u) = {}_2\tilde{F}_1\left[+\frac{1}{2}, +\frac{1}{2}; \frac{d}{2}; \frac{u^2}{(u+1)^2}\right], \tag{A12}$$

$$G_{11}(d,u) = {}_2\tilde{F}_1\left[-\frac{1}{2}, +\frac{3}{2}; \frac{d+2}{2}; \frac{u^2}{(u+1)^2}\right], \tag{A13}$$

where ${}_2F_1$ denotes an ordinary hypergeometric function and ${}_2\tilde{F}_1$ for a regularized hypergeometric function. Furthermore, the $G_0^{(i)}(d,u)$ functions from (A2) are given as

$$G_0^{(2)} = \frac{\pi^{3/2}(d-2)[3d(u+1)+u+9]\,\Gamma\left(\frac{d}{2}\right)}{128(d^2+d-2)(u+1)^3\Gamma\left(\frac{d+3}{2}\right)}, \tag{A14}$$

$$G_0^{(3)} = -\frac{\pi^{3/2}(d-2)[(d-3)u+d+5]\,\Gamma\left(\frac{d}{2}\right)}{64(d-1)(d+2)(u+2)^3\Gamma\left(\frac{d+3}{2}\right)}, \tag{A15}$$

$$G_0^{(4)} = -\frac{\pi^{3/2}(d-2)[(d+7)u+d-1]\,\Gamma\left(\frac{d}{2}\right)}{128(d^2+d-2)(u+1)^3\Gamma\left(\frac{d+3}{2}\right)}. \tag{A16}$$

The remaining functions $g_j^{(i)}$ with $i \in 2,3,4$ and $j \in 1,\ldots,11$ are defined for $i = 2$ as

$$g_1^{(2)} = \frac{\pi^2\, 2^{-d-7}\, P_{2,1}\, \Gamma(d-1)}{(u+1)^3\Gamma\left(\frac{d}{2}+2\right)\Gamma\left(\frac{d}{2}\right)}, \tag{A17}$$

$$g_2^{(2)} = -\frac{\pi^2\, 2^{-d-9} P_{2,2}\, \Gamma(d+3)}{(d-1)(d+1)^2 u(u+1)^4(2u+1)\Gamma\left(\frac{d}{2}+2\right)^2}, \tag{A18}$$

$$g_3^{(2)} = -\frac{\pi^2\, 2^{-d-10}\, P_{2,3}\, \Gamma(d+3)}{(d-1)(d+1)^2 u(u+1)^2(2u+1)^2\Gamma\left(\frac{d}{2}+2\right)^2}, \tag{A19}$$

$$g_4^{(2)} = \frac{\pi^2\, 2^{-d-8}\, P_{2,4}\, \Gamma(d-1)}{u(u+1)^2(2u+1)^2\Gamma\left(\frac{d}{2}+2\right)\Gamma\left(\frac{d}{2}\right)}, \tag{A20}$$

$$g_5^{(2)} = \frac{\pi^2\, 2^{-d-7}\, P_{2,5}\, \Gamma(d-1)}{(u+1)^2(2u+1)\Gamma\left(\frac{d}{2}+1\right)\Gamma\left(\frac{d}{2}+2\right)}, \tag{A21}$$

$$g_6^{(2)} = \frac{3\pi^2\, 2^{-d-7}\, P_{2,6}\, \Gamma(d-1)}{(u+1)^2\Gamma\left(\frac{d}{2}+2\right)^2}, \tag{A22}$$

$$g_7^{(2)} = -\frac{\pi^2\, 2^{-d-7}\, P_{2,7}\, \Gamma(d-1)}{(u+1)^3(2u+1)\Gamma\left(\frac{d}{2}+1\right)\Gamma\left(\frac{d}{2}+2\right)}, \tag{A23}$$

$$g_8^{(2)} = -\frac{\pi^{3/2}\, P_{2,8}\, \Gamma\left(\frac{d-1}{2}\right)}{1024 d(u+1)^5\Gamma\left(\frac{d}{2}+2\right)}, \tag{A24}$$

$$g_9^{(2)} = \frac{9\pi^{3/2}\, P_{2,9}\, \Gamma\left(\frac{d-1}{2}\right)}{64 d^2(d+2)^2(u+1)^4\Gamma\left(\frac{d}{2}\right)}, \tag{A25}$$

$$g_{10}^{(2)} = \frac{\pi^2\, 2^{-d-7}\, P_{2,10}\, \Gamma(d+1)}{(d-1)(u+1)^3\Gamma\left(\frac{d}{2}+2\right)}, \tag{A26}$$

$$g_{11}^{(2)} = \frac{3\pi^{3/2}\, P_{2,11}\, \Gamma\left(\frac{d-1}{2}\right)}{64 d(d+2)(u+1)}, \tag{A27}$$

where the polynomials $P_{2,j}$ with $j \in 1,\ldots,11$ over u and d have been singled out and are given in the text below. Analogously to the $i = 2$ case we get for $i = 3$ the following expressions:

$$g_1^{(3)} = \frac{\pi^{3/2}\, P_{3,11}\, \Gamma\left(\frac{d-1}{2}\right)}{512(u+1)^3\Gamma\left(\frac{d}{2}+2\right)}, \tag{A28}$$

$$g_2^{(3)} = -\frac{\pi^2 2^{-d-8}\, P_{3,10}\, \Gamma(d+3)}{(d-1)(d+1)^2 u(u+1)^4(2u+1)\Gamma\left(\frac{d}{2}+2\right)^2}, \tag{A29}$$

$$g_3^{(3)} = -\frac{\pi^2 2^{-d-9}\, P_{3,9}\, \Gamma(d+3)}{(d-1)(d+1)^2 u(u+1)^2(2u+1)^2\Gamma\left(\frac{d}{2}+2\right)^2},$$

$$g_4^{(3)} = \frac{\pi^2 2^{-d-7}\, P_{3,8}\, \Gamma(d-1)}{u(u+1)^2(2u+1)^2\Gamma\left(\frac{d}{2}+2\right)\Gamma\left(\frac{d}{2}\right)}, \tag{A30}$$

$$g_5^{(3)} = \frac{\pi^2 2^{-d-8}\, P_{3,7}\, \Gamma(d-1)}{(u+1)^2(2u+1)\Gamma\left(\frac{d}{2}+2\right)^2}, \tag{A31}$$

$$g_6^{(3)} = \frac{\pi^2 2^{-d-7}\, P_{3,6}\, \Gamma(d-1)}{(u+1)^2\Gamma\left(\frac{d}{2}+2\right)^2}, \tag{A32}$$

$$g_7^{(3)} = -\frac{\pi^2 2^{-d-8}\, P_{3,5}\, \Gamma(d-1)}{(u+1)^3(2u+1)\Gamma\left(\frac{d}{2}+2\right)^2}, \tag{A33}$$

$$g_8^{(3)} = -\frac{\pi^{3/2}\, P_{3,4}\, \Gamma\left(\frac{d-1}{2}\right)}{512 d(u+1)^5\Gamma\left(\frac{d}{2}+2\right)}, \tag{A34}$$

$$g_9^{(3)} = -\frac{3\pi^{3/2} u^2\, P_{3,3}\, \Gamma\left(\frac{d-1}{2}\right)}{32 d^2(d+2)^2(u+1)^4\Gamma\left(\frac{d}{2}\right)}, \tag{A35}$$

$$g_{10}^{(3)} = \frac{\pi^2 2^{-d-7}\, P_{3,2}\, \Gamma(d+1)}{(d-1)(u+1)^3\Gamma\left(\frac{d}{2}+2\right)}, \tag{A36}$$

$$g_{11}^{(3)} = \frac{\pi^{3/2}\, P_{3,1}\, \Gamma\left(\frac{d-1}{2}\right)}{32(d+2)(u+1)}, \tag{A37}$$

where the polynomials $P_{3,j}$ with $j \in 1,\ldots,11$ over u and d have been singled out and are given in the text below. Analogously to the $i = 2,3$ cases we get for $i = 4$ the following expressions:

$$g_1^{(4)} = \frac{\pi^2 2^{-d-7}\, P_{4,1}\, \Gamma(d-1)}{(u+1)^3\Gamma\left(\frac{d}{2}+2\right)\Gamma\left(\frac{d}{2}\right)}, \tag{A38}$$

$$g_2^{(4)} = -\frac{\pi^2 2^{-d-5}\, P_{4,2}\, \Gamma(d-1)}{d(d+1)(d+2)u(u+1)^4(2u+1)\Gamma\left(\frac{d}{2}\right)^2}, \tag{A39}$$

$$g_3^{(4)} = -\frac{\pi^2 2^{-d-6}\, P_{4,3}\, \Gamma(d-1)}{d(d+1)(d+2)u(u+1)^2(2u+1)^2\Gamma\left(\frac{d}{2}\right)^2}, \tag{A40}$$

$$g_4^{(4)} = \frac{\pi^{3/2}\, P_{4,4}\, \Gamma\left(\frac{d-1}{2}\right)}{1024 u(u+1)^2(2u+1)^2\Gamma\left(\frac{d}{2}+2\right)}, \tag{A41}$$

$$g_5^{(4)} = \frac{\pi^{3/2}\, P_{4,5}\, \Gamma\left(\frac{d-1}{2}\right)}{128 d(u+1)^2(2u+1)\Gamma\left(\frac{d}{2}+2\right)}, \tag{A42}$$

$$g_6^{(4)} = -\frac{\pi^2 2^{-d-7}\, P_{4,6}\, \Gamma(d-1)}{(u+1)^2\Gamma\left(\frac{d}{2}+2\right)^2}, \tag{A43}$$

$$g_7^{(4)} = -\frac{\pi^{3/2}\, P_{4,7}\, \Gamma\left(\frac{d-1}{2}\right)}{128 d(u+1)^3(2u+1)\Gamma\left(\frac{d}{2}+2\right)}, \tag{A44}$$

$$g_8^{(4)} = \frac{\pi^{3/2} u\, P_{4,8}\, \Gamma\left(\frac{d-1}{2}\right)}{1024 d(u+1)^5\Gamma\left(\frac{d}{2}+2\right)}, \tag{A45}$$

$$g_9^{(4)} = -\frac{3\pi^{3/2} u^2\, P_{4,9}\, \Gamma\left(\frac{d-1}{2}\right)}{32 d^2(d+2)^2(u+1)^4\Gamma\left(\frac{d}{2}-1\right)}, \tag{A46}$$

$$g_{10}^{(4)} = 0, \tag{A47}$$

$$g_{11}^{(4)} = \frac{\pi^{3/2}\, P_{4,11}\, \Gamma\left(\frac{d-1}{2}\right)}{64(d+2)(u+1)}, \tag{A48}$$

where the polynomials $P_{4,j}$ with $j \in 1,\ldots,11$ over u and d have been singled out and are given together with $P_{2,j}$ and $P_{3,j}$ for $j \in 1,\ldots,11$ now in the text below. Let us start with the polynomials for $i = 2$. We obtain the following expressions:

$$P_{2,1} = d^2(7u^2+4u) - 3d(6u^2+5u) + 8u^2 - 22u - 30, \tag{A49}$$

$$\begin{aligned} P_{2,2} = {} & 2d^4(7u+6)(u+1)^5 - d^3(u+1)^2(119u^4+347u^3 \\ & + 384u^2 + 191u + 33) + d^2(117u^6 + 751u^5 \\ & + 1733u^4 + 1694u^3 + 720u^2 + 74u - 19) \\ & + d(190u^6 + 82u^5 + 210u^4 + 1004u^3 + 1389u^2 \\ & + 765u + 146) - 8(2u+1)(u+1)^2(5u^3 - 19u^2 \\ & + 48u + 18), \end{aligned} \tag{A50}$$

$$\begin{aligned} P_{2,3} = {} & 2d^5(6u+5)(u+1)^5 + d^4(u+1)^2(19u^4 - 140u^3 \\ & - 408u^2 - 318u - 73) - d^3(41u^6 + 16u^5 - 251u^4 \\ & - 750u^3 - 545u^2 - 54u + 31) - d^2(76u^6 + 3291u^4 \\ & + 2656u^3 - 370u^2 - 1006u - 253) + d(-28u^6 \\ & + 1954u^5 + 3757u^4 + 2548u^3 + 76u^2 - 410u - 81) \\ & + 2(2u+1)(45u^4 + 636u^3 + 1236u^2 + 656u + 123), \end{aligned} \tag{A51}$$

$$\begin{aligned} P_{2,4} = {} & 2d^4(6u+5)(u+1)^5 - d^3(1+u)^2(5u^4 + 152u^3 \\ & + 352u^2 + 260u + 59) - d^2(31u^6 + 258u^5 + 606u^4 \\ & + 358u^3 + 101u^2 + 96u + 38) - d(14u^6 - 714u^5 \\ & - 1419u^4 - 1934u^3 - 2166u^2 - 1240u - 253) \\ & - 2(2u+1)(7u^4 - 150u^3 - 252u^2 - 10u + 21), \end{aligned} \tag{A52}$$

$$\begin{aligned} P_{2,5} = {} & d^2(d-2)(8u^3 + 19u^2 + 14u + 3) \\ & - d(d-2)(122u^3 + 209u^2 + 102u + 15) \\ & + (d-2)(30u^3 - 196u^2 - 188u - 42), \end{aligned} \tag{A53}$$

$$\begin{aligned} P_{2,6} = {} & d^2(d+2)(1+3u+2u^2) \\ & - d(d+2)(3+4u+5u^2) - 8(d+2)u, \end{aligned} \tag{A54}$$

$$\begin{aligned} P_{2,7} = {} & d^2(d-2)(8u+3)(u+1)^3 \\ & - 2d(d-2)(u+1)(37u^3 + 56u^2 + 24u + 3) \\ & + 8(d-2)(2u+1)(2u^3 - 6u^2 - 10u - 3), \end{aligned} \tag{A55}$$

$$\begin{aligned} P_{2,8} = {} & 2d^2(u+1)^2(3u^2+5u+6) + d(43u^4 + 155u^3 \\ & + 155u^2 + 49u) - 14u^4 - 6u^3 + 110u^2 \\ & + 150u + 48, \end{aligned} \tag{A56}$$

$$P_{2,9} = u^2[d(5u+1) - 2u + 6], \tag{A57}$$

$$P_{2,10} = d(10u+7), \tag{A58}$$

$$P_{2,11} = (3d+2u), \tag{A59}$$

$$P_{3,1} = u[(d-2)(d+16)u + 4(3d-8)], \tag{A60}$$

$$\begin{aligned} P_{3,2} = {} & 2d^4(u+1)^6 - d^3(u+1)^2(6u^4 + 22u^3 + 35u^2 \\ & + 28u + 8) - d^2(2u+1)(54u^5 + 129u^4 + 78u^3 \\ & + 4u^2 - 27u - 12) + d(u+1)(108u^5 + 466u^4 \\ & + 700u^3 + 474u^2 + 149u + 18) + 4(2u+1) \\ & \times (u+1)^2(26u^3 - 24u^2 - 41u - 13), \end{aligned} \tag{A61}$$

$$\begin{aligned} P_{3,3} = {} & d^5(4u+3)(u+1)^5 + d^4(u+1)^2(19u^4 + u^3 \\ & - 76u^2 - 76u - 20) + d^3(7u^6 - 268u^5 - 938u^4 \\ & - 1002u^3 - 449u^2 - 82u - 4) - d^2(52u^6 + 170u^5 \\ & + 139u^4 - 453u^3 - 613u^2 - 253u - 34) - d(44u^6 \\ & + 210u^5 + 129u^4 - 134u^3 - 176u^2 - 76u - 13) \\ & + 2(2u+1)(175u^4 + 572u^3 + 610u^2 + 276u + 47), \end{aligned} \tag{A62}$$

$$\begin{aligned} P_{3,4} = {} & d^4(4u+3)(u+1)^5 + d^3(u+1)^2(11u^4 - 13u^3 \\ & - 80u^2 - 73u - 19) - d^2(15u^6 + 304u^5 + 905u^4 \\ & + 904u^3 + 379u^2 + 60u + 1) - d(22u^6 - 106u^5 \\ & - 771u^4 - 1396u^3 - 1104u^2 - 410u - 59) \\ & + 2(2u+1)(u+1)^2(67u^2 + 22u - 5), \end{aligned} \tag{A63}$$

$$\begin{aligned} P_{3,5} = {} & (d^2-4)[d(u+1) - 15u - 7][4(d+4)u^2 \\ & + (5d+14)u + d + 2], \end{aligned} \tag{A64}$$

$$\begin{aligned} P_{3,6} = {} & d^2(d+2)(u+1)(2u+1) - 2d(d+2)(5u+1) \\ & - 4(d+2)u(7u+3), \end{aligned} \tag{A65}$$

$$\begin{aligned} P_{3,7} = {} & d^2(d-2)(d+2)\big[(4u+1)(u+1)^3 \\ & - 2d(u+1)(4u^3 + 11u^2 + 6u + 1) \\ & - 8(2u+1)(10u^3 + 15u^2 + 8u + 1)\big], \end{aligned} \tag{A66}$$

$$\begin{aligned} P_{3,8} = {} & d^2(u+2)(u+1)^3 - du(13u^3 + 51u^2 + 53u + 17) \\ & + 2(u+1)(19u^3 + 54u^2 + 31u + 4), \end{aligned} \tag{A67}$$

$$P_{3,9} = d(5u+1) - 14u - 6, \tag{A68}$$

$$P_{3,10} = d(2u+1), \tag{A69}$$

$$P_{3,11} = 5u + 1, \tag{A70}$$

$$P_{4,1} = (d-2)(4u^2+5u) - 2, \tag{A71}$$

$$\begin{aligned} P_{4,2} = {} & d^3(u+1)^4(13u^2 + 15u + 1) - d^2(u+1)(109u^5 \\ & + 366u^4 + 505u^3 + 335u^2 + 91u + 5) + d(54u^6 \\ & + 970u^5 + 2150u^4 + 2110u^3 + 1007u^2 + 205u + 10) \\ & + 8(2u+1)(u+1)^2(11u^3 - 39u^2 - 19u - 1), \end{aligned} \tag{A72}$$

$$\begin{aligned} P_{4,3} = {} & d^4(u+1)^4(19u^2 + 16u + 1) + d^3(35u^4 - 254u^3 \\ & - 422u^2 - 160u - 9)(u+1)^2 - d^2(28u^6 + 454u^5 \\ & - 265u^4 - 1534u^3 - 1164u^2 - 288u - 15) - d(44u^6 \end{aligned}$$

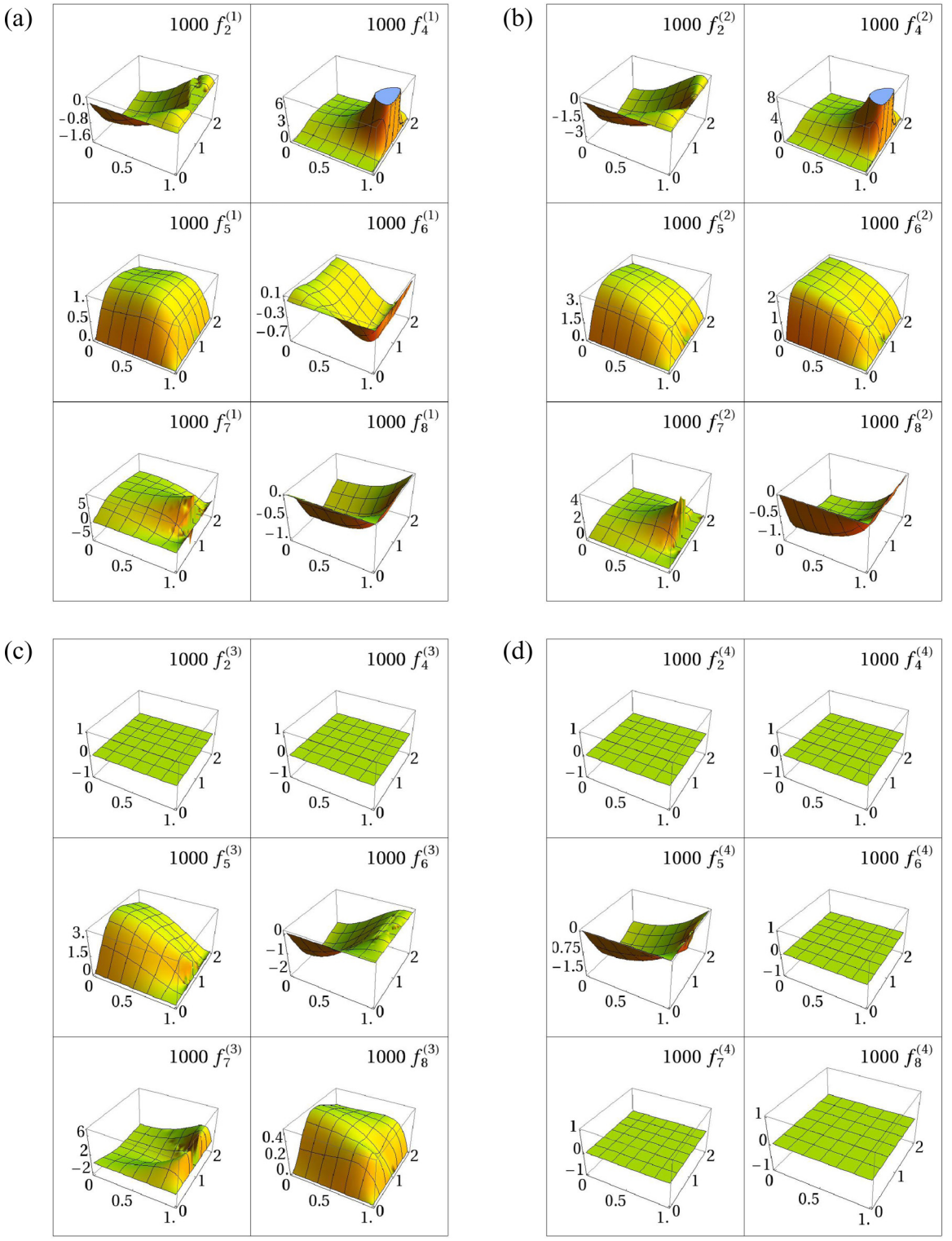

FIG. 8. Functions $f_l^{(i)}$ for $l \in 2,4,5,6,7,8$ and $i \in 1,2,3,4$ shown for u corresponding to a value typical of the $A = -1$ model. Values of $f^{(0)}$ have already been determined within the scope of the $A = 0$ model in Ref. [11]. (a) depicts coefficients $f_l^{(1)}$, (b) shows $f_l^{(2)}$, (c) shows $f_l^{(i)}$, and (d) shows $f_l^{(4)}$. Note that only the fifth graph actually contributes terms of order A^4 to the final expression for $z_{21}^{(2)}$ since all the other graphs contribute zero coefficients $f_l^{(4)}$, as shown by flat planes in the corresponding figures. All dependencies are plotted in the region of $x \in \langle 0,1 \rangle$ and $z \in \langle 0,2 \rangle$.

$$+1630u^5+2699u^4+2272u^3+1004u^2+190u+9)$$
$$+2(2u+1)(485u^4+1084u^3+664u^2+152u+7), \quad \text{(A73)}$$

$$P_{4,4}=d^3[u(19u+16)+1](u+1)^4-d^2(u+1)^2(3u^4$$
$$+272u^3+389u^2+144u+8)-d(22u^6+430u^5$$
$$-175u^4-1290u^3-1018u^2-260u-13)$$
$$+2(2u+1)(113u^4+226u^3+32u^2-18u-1), \quad \text{(A74)}$$

$$P_{4,5}=(d-2)u(5u+2)[\,(d-15)u+d-7\,], \quad \text{(A75)}$$

$$P_{4,6}=(d+2)(5u+1)(d+2u), \quad \text{(A76)}$$

$$P_{4,7}=(d-2)u\big[d(u+1)^2(5u+2)-4(2u+1)(4u^2$$
$$+7u+2)], \quad \text{(A77)}$$

$$P_{4,8}=d(17u^3+49u^2+49u+15)-2(u+1)^2(17u+15), \quad \text{(A78)}$$

$$P_{4,9}=5u+1, \quad \text{(A79)}$$

$$P_{4,10}=0, \quad \text{(A80)}$$

$$P_{4,11}=5u+1. \quad \text{(A81)}$$

Let us turn our attention to the remaining seven diagrams of Fig. 3. Instead of calculating the graphs using the previously discussed technique of Ref. [9], we have employed the derivative technique outlined by the authors of Ref. [15], as it allows an easy algorithmic approach. By analogy with Eq. (A1), for each diagram $l\in 2,\ldots,8$ we may explicitly determine every coefficient of the resulting polynomial over A separately for each graph. The corresponding decomposition reads as now

$$B_l^{(\rho)}=16u(1-x^2)^{\frac{1-d}{2}}\int_1^\infty\frac{dz}{z}\sum_{i=0}^{4}A^i\,f_l^{(i)}(x,z) \quad \text{(A82)}$$

with $l\in 2,\ldots,8$. Notice that contrary to expression (A1), integrations over variables $x\in\langle -1,1\rangle$ with $x=\mathbf{k}\cdot\mathbf{q}/|k|/|q|$ and $z\geqslant 1$ are singled out. Each of the functions $f_l^{(i)}(x,z,u,d)$ is a rational function over x, z, u, and d. Since for $l\in 2,4,5,6,7,8$ the corresponding expressions are lengthy and require a huge amount of space, we do not show the explicit form of their corresponding $f_l^{(i)}$ functions. Instead, as an example, we give now the corresponding expressions only for the third two-loop diagram $\Gamma_3^{(2)}$ of Fig. 3 and present the remaining functions $f_l^{(i)}$ for $l\in 2,4,5,6,7,8$ graphically in Fig. 7. Since the $A=0$ case was completely solved in Ref. [11], we now present only $f_3^{(1)}(x,z,u,d)$ and $f_3^{(2)}(x,z,u,d)$. As discussed in the main body of the article, for the present diagram $f_3^{(3)}(x,z,u,d)=f_3^{(4)}(x,z,u,d)=0$ because of the structure of A polynomials. Thus, we get

$$f_3^{(1)}=\frac{(-2+d)(d-2u+du)z(1+z^2)}{16(-1+d)d(2+d)(1+u)^2(-1+xz-z^2)}$$
$$\times\frac{-(1+z^2)^2+x^2(3-2z^2+3z^4)}{(-1+2xz-z^2)(1+xz+z^2)(1+2xz+z^2)}, \quad \text{(A83)}$$

$$f_3^{(2)}=\frac{(-2+d)(1+3u)z(1+z^2)}{16(-1+d)d(2+d)(1+u)^2(-1+xz-z^2)}$$
$$\times\frac{-(1+z^2)^2+x^2(3-2z^2+3z^4)}{(-1+2xz-z^2)(1+xz+z^2)(1+2xz+z^2)}. \quad \text{(A84)}$$

As already discussed, the graph $\Gamma_3^{(2)}$ contains only two V_{ijl} type vertices and its corresponding functions $f_3^{(3)}(x,z,u,d)$ and $f_3^{(4)}(x,z,u,d)$, which correspond to polynomial coefficients in front of A^3 and A^4, respectively, are both zero. For the remaining graphs $\Gamma_l^{(2)}$ with $l\in 2,4,5,6,7,8$ the $f_l^{(i)}(x,z,u,d)$ functions with $i\in 0,\ldots,4$ are lengthy and require a huge amount of space and we shall only present them graphically via Fig. 8 for $u=1$ which presents the usual order of this parameter value, as used in calculations of the turbulent Prandtl number via Eq. (49).

[1] A. Yoshizawa, S. I. Itoh, and K. Itoh, *Plasma and Fluid Turbulence: Theory and Modelling* (IoP, Bristol, 2003).

[2] D. Biskamp, *Magnetohydrodynamic Turbulence* (Cambridge University Press, Cambridge, 2003).

[3] A. S. Monin and A. M. Yaglom, *Statistical Fluid Mechanics* (MIT Press, Cambridge, MA, 1975), Vol. 2.

[4] W. D. McComb, *The Physics of Fluid Turbulence* (Clarendon, Oxford, 1990).

[5] B. I. Shraiman and E. D. Siggia, Rev. Nat. **405**, 639 (2000).

[6] J. M. Coulson and J. F. Richardson, *Chemical Engineering* (Elsevier, Amsterdam, 1999), Vol. 1.

[7] L. P. Chua and R. A. Antonia, Int. J. Heat Mass Transfer **33**, 331 (1990).

[8] L. P. Chang and E. A. Cowen, J. Eng. Mech. **128**, 1082 (2002).

[9] A. N. Vasilev, *Quantum-Field Renormalization Group in the Theory of Critical Phenomena and Stochastic Dynamics* (CRC Press, Boca Raton, FL, 2004).

[10] L. T. Adzhemyan, N. V. Antonov, and A. N. Vasilev, *The Field Theoretic Renormalization Group in Fully Developed Turbulence* (Gordon & Breach, London, 1999).

[11] E. Jurčišinová, M. Jurčišin, and P. Zalom, Phys. Rev. E **89**, 043023 (2014).

[12] N. V. Antonov and N. M. Gulitskiy, Phys. Rev. E **91**, 013002 (2015).

[13] N. V. Antonov and N. M. Gulitskiy, Phys. Rev. E **92**, 043018 (2015).

[14] E. Jurčišinová, M. Jurčišin, and R. Remecký, Phys. Rev. E **93**, 033106 (2016).
[15] L. T. Adzhemyan, J. Honkonen, T. L. Kim, and L. Sladkoff, Phys. Rev. E **71**, 056311 (2005).
[16] L. T. Adzhemyan, N. V. Antonov, A. Mazzino, P. Muratore-Ginanneschi, and A. V. Runov, Europhys. Lett. **55**, 801 (2001).
[17] N. V. Antonov, M. Hnatich, J. Honkonen, and M. Jurčišin, Phys. Rev. E **68**, 046306 (2003).
[18] P. C. Hohenberg and B. I. Halperin, Rev. Mod. Phys. **49**, 435 (1977).
[19] D. Forster, D. R. Nelson, and M. J. Stephen, Phys. Rev. Lett. **36**, 867 (1976).
[20] D. Forster, D. R. Nelson, and M. J. Stephen, Phys. Rev. A **16**, 732 (1977).
[21] H. Arponen, Phys. Rev. E **79**, 056303 (2009).
[22] J. Zinn-Justin, *Quantum Field Theory and Critical Phenomena* (Clarendon, Oxford, 1989).
[23] L. T. Adzhemyan, A. N. Vasilev, and Yu. M. Pismak, Theor. Math. Phys. **57**, 1131 (1983).
[24] L. T. Adzhemyan, N. V. Antonov, M. V. Kompaniets, and A. N. Vasilev, Int. J. Mod. Phys. B **17**, 2137 (2003).
[25] L. T. Adzhemyan, J. Honkonen, M. V. Kompaniets, and A. N. Vasilev, Phys. Rev. E **68**, 055302(R) (2003).
[26] L. T. Adzhemyan, A. N. Vasilev, and M. Gnatich, Theor. Math. Phys. **74**, 180 (1988).
[27] L. T. Adzhemyan, N. V. Antonov, and A. N. Vasilev, Usp. Fiz. Nauk **166**, 1257 (1996) [Phys. Usp. **39**, 1193 (1996)].
[28] L. T. Adzhemyan, J. Honkonen, M. V. Kompaniets, and A. N. Vasilev, Phys. Rev. E **71**, 036305 (2005).
[29] L. T. Adzhemyan, J. Honkonen, T. L. Kim, M. V. Kompaniets, L. Sladkoff, and A. N. Vasil'ev, J. Phys. A: Math. Gen. **39**, 7789 (2006).
[30] L. T. Adzhemyan, A. N. Vasilev, and M. Gnatich, Theor. Math. Phys. **58**, 47 (1984).
[31] L. T. Adzhemyan, N. V. Antonov, and A. N. Vasilev, Phys. Rev. E **58**, 1823 (1998).
[32] L. T. Adzhemyan, N. V. Antonov, V. A. Barinov, Y. S. Kabrits, and A. N. Vasilev, Phys. Rev. E **63**, 025303(R) (2001); **64**, 019901(E) (2001).
[33] S. V. Novikov, Theor. Math. Phys. **136**, 936 (2003).
[34] N. V. Antonov and M. M. Kostenko, Phys. Rev. E **90**, 063016 (2014).
[35] C. Pagani, Phys. Rev. E **92**, 033016 (2015).
[36] L. T. Adzhemyan, A. N. Vasilev, and M. Gnatich, Theor. Math. Phys. **64**, 777 (1985).
[37] L. T. Adzhemyan, A. N. Vasilev, and M. Hnatich, Theor. Math. Phys. **72**, 940 (1987).
[38] N. V. Antonov and M. M. Kostenko, Phys. Rev. E **92**, 053013 (2015).
[39] E. Jurčišinová, M. Jurčišin, and R. Remecký, Phys. Rev. E **84**, 046311 (2011).
[40] E. Jurčišinová, M. Jurčišin, R. Remecký, and P. Zalom, Phys. Rev. E **87**, 043010 (2013).
[41] L. T. Adzhemyan, N. V. Antonov, P. B. Goldin, and M. V. Kompaniets, J. Phys. A: Math. Theor. **46**, 135002 (2013); N. V. Antonov and N. M. Gulitskiy, Theor. Math. Phys. **176**, 851 (2013).
[42] S. V. Novikov, J. Phys. A: Math. Gen. **39**, 8133 (2006).
[43] H. Arponen, Phys. Rev. E **81**, 036325 (2010).
[44] E. Jurčišinová, M. Jurčišin, and R. Remecký, Phys. Rev. E **88**, 011002(R) (2013).
[45] P. C. Martin, E. D. Siggia, and H. A. Rose, Phys. Rev. A **8**, 423 (1973); C. De Dominicis, J. Phys. (Paris), Colloq. **37**, C1-247 (1976); H. K. Janssen, Z. Phys. B **23**, 377 (1976); R. Bausch, H. K. Janssen, and H. Wagner, *ibid.* **24**, 113 (1976).
[46] J. C. Collins, *Renormalization: An Introduction to Renormalization, the Renormalization Group and the Operator-Product Expansion* (Cambridge University Press, Cambridge, 1986).
[47] S. S. Moiseev, R. Z. Sagdeev, A. V. Tur, G. A. Khomenko, and V. V. Yanovskii, Zh. Eksp. Teor. Fiz. **85**, 1979 (1983) [JETP **58**, 1149 (1983)].
[48] A. Pouquet, J. D. Fournier, and P. L. Sulem, J. Phys. Lett. (Paris), **39L**, 199 (1978).
[49] S. I. Vainshtein, Ya. B. Zel'dovich, and A. A. Ruzmaikin, *The Turbulent Dynamo in Astrophysics* (in Russian) (Nauka, Moscow, 1980); S. I. Vainshtein, *Magnetic Fields in Space* (in Russian) (Nauka, Moscow, 1983).
[50] H. K. Moffat, *Magnetic Field Generation in Electrically Conducting Fluids* (Cambridge University Press, Cambridge, 1978).
[51] A. A. Migdal, Mod. Phys. Lett. A **06**, 1023 (1991).
[52] L. T. Adzhemyan, M. Hnatich, and M. Stehlik, J. Phys. II (France) **5**, 1077 (1995).
[53] L. T. Adzhemyan, M. Hnatich, and M. V. Kompaniets, Theor. Math. Phys. **176**, 835 (2013).
[54] J. D. Fournier and U. Frisch, Phys. Rev. A **28**, 1000 (1983).
[55] L. T. Adzhemyan, A. N. Vasil'ev, and M. Gnatich, Theor. Math. Phys. **58**, 47 (1984).